Published in final edited form as:
Contrast Media Mol Imaging. 2014 January ; 9(1): 37–52. doi:10.1002/cmmi.1551.

Nanoparticle Contrast Agents for Computed Tomography: A Focus on Micelles

David P. Cormode[1,*], **Pratap C. Naha**[1], and **Zahi A. Fayad**[2]

[1] Departments of Radiology, Cardiology and Bioengineering, University of Pennsylvania, 3400 Spruce St, 1 Silverstein, Philadelphia, PA 19104, USA

[2] Translational and Molecular Imaging Institute, Mount Sinai School of Medicine, New York, NY.

Abstract

Computed tomography (CT) is an X-ray based whole body imaging technique that is widely used in medicine. Clinically approved contrast agents for CT are iodinated small molecules or barium suspensions. Over the past seven years there has been a great increase in the development of nanoparticles as CT contrast agents. Nanoparticles have several advantages over small molecule CT contrast agents, such as long blood-pool residence times, and the potential for cell tracking and targeted imaging applications. Furthermore, there is a need for novel CT contrast agents, due to the growing population of renally impaired patients and patients hypersensitive to iodinated contrast. Micelles and lipoproteins, a micelle-related class of nanoparticle, have notably been adapted as CT contrast agents. In this review we discuss the principles of CT image formation and the generation of CT contrast. We discuss the progress in developing non-targeted, targeted and cell tracking nanoparticle CT contrast agents. We feature agents based on micelles and used in conjunction with spectral CT. The large contrast agent doses needed will necessitate careful toxicology studies prior to clinical translation. However, the field has seen tremendous advances in the past decade and we expect many more advances to come in the next decade.

Keywords

nanoparticle; micelle; computed tomography; X-ray; spectral CT; iodine; gold nanoparticle; lipoprotein; molecular imaging; bismuth

1 Introduction

The currently approved computed tomography (CT) contrast agents for intravenous injection are iodinated small molecules.(1) For example, iohexol has a benzene core with three iodine atoms for CT contrast and three amide and six alcohol groups for water solubility and low osmolality (Figure 1A). These iodine contrast agents have a short blood half-life, but are excellent for a number of clinical applications such as vascular imaging, due to the fast scanning speed of CT.(2) Nevertheless, a wide range of elements give good CT contrast(3) and a number of types of formulations have been proposed as alternative CT contrast agents over the years such as gadolinium chelates or tungsten clusters.(4,5) Nanoparticle contrast agents for CT were developed as early as the 1980s,(6-10) but such reports were infrequent and the area did not grow.(11) Notably, two of these agents were trialed in the clinic, but were not further pursued due to non-tolerable side effects.(12) Nevertheless, in the past five years the field has again attracted significant interest, as evidenced by rapid growth in the

* Corresponding Author Tel: 215-746-1382, Fax: 240-368-8096 david.cormode@uphs.upenn.edu.

number of publications and citations on nanoparticle contrast agents for CT, with over one hundred publications and twenty five hundred citations on the topic from 2012 alone (Figure 1B,C).

Nanoparticles are tiny particles that have one or more dimensions in the nanoscale, i.e. from 1-100 nm. They are frequently spheres, but can have many other shapes, such as rods, cages or stars.(13-15) Nanoparticles are now widely used in medicinal applications, a field known as nanomedicine.(16) They can be used as therapeutics: Doxil is a liposomal formulation of doxorubicin that is FDA approved for the treatment of certain cancers, for example.(17) Other therapeutic applications for nanoparticles include siRNA delivery or thermal ablation.(18,19) Nanoparticles are also used as tracers or contrast agents for a variety of medical imaging methods, such as PET, MRI, photoacoustics and fluorescence imaging. Iron oxide nanoparticles have been FDA approved for MRI since the mid-1990's.(20) There are several reasons for this interest in nanoparticles. In general, nanoparticles carry a high payload of contrast generating material compared with small molecules.(21) Also, some nanoparticles, such as iron oxides or quantum dots, yield contrast that cannot be produced by small molecules.(20,22) Depending on the properties of their coating material, nanoparticles can have long blood circulation half-lives.(23) Last, multiple properties/components can be integrated into nanoparticles with relative ease.(24) For example, for some types of nanoparticles, to incorporate additional functionalities simply requires their addition to the synthesis feedstocks, with no extra steps required.(25)

The knowledge acquired from applying nanoparticles in these other biomedical settings is now being applied to the development of contrast agents for computed tomography.(26) A schematic of a nanoparticle contrast agent designed for CT is depicted in Figure 1D. The material used to generate contrast for CT is usually in the core of the particle. The contrast generating element used is most frequently iodine,(27) gold,(28) or bismuth,(29) but the use of various elements such as bromine,(30) tantalum,(31) platinum,(32) ytterbium,(33) yttrium,(34) gadolinium(35,36), tungsten(1) and others has been reported. The core is coated with a polymer, lipid, protein, silica or other compounds that yield solubility in biological media and biocompatibility. The coating can be modified in various ways to include targeting moieties (antibodies, proteins, peptides, aptamers and so forth).(37-40) Sources of contrast for other imaging techniques, such as fluorophores for fluorescent imaging or gadolinium chelates for MR contrast may also be loaded into the nanoparticle.(28,41) Last, the coating or core can also be loaded with drugs or nucleic acid to create so-called ‘theranostic’ nanoparticles (both therapeutically and diagnostically active).(42,43) A variety of nanoparticle types have been used as contrast agents for CT, such as emulsions, liposomes, micelles, lipoproteins, polymeric nanoparticles, solid metal nanoparticles and so on. Micelles and lipoproteins, which can be regarded as a form of micelle, have yielded excellent results as CT contrast agents.(28,44-48)

Nanoparticle contrast agents for CT have several exciting applications. As mentioned above, a feature of nanoparticles is that their circulation half-lives have been reported to be as long as 15 hours, whereas that of iodinated molecules is only minutes.(49) CT contrast agents that circulate for a long time(50) could be used in applications where repeated injection of iodine contrast agents is required, such as for stent placement. Nanoparticles can be used to allow cell tracking in vivo.(51) Targeted nanoparticle CT contrast agents can detect the expression of proteins or cell types in tissues, for example detecting the macrophage content of atherosclerotic plaque.(44) Nanoparticles can also be used with emerging CT techniques, such as spectral CT, which can specifically detect exogenous contrast agents.(52) Additionally, nanoparticles can be multifunctional and so can provide contrast for multiple imaging modalities, e.g. CT, MRI and fluorescence,(28) or provide therapeutic effects as well as CT contrast.(19) Last, nanoparticles may be compatible with patients for whom

conventional iodinated contrast media is contraindicated due to renal insufficiency or allergic responses.(53)

In the following sections we will outline the process of CT image formation, the physics of CT contrast and give recommendations for the evaluation of the contrast produced by novel media. We will discuss nanoparticle structure/types and the development of nanoparticle CT contrast agents over the past thirty years. We will focus on examples of long circulating agents, targeted agents, cell tracking, agents used in conjunction with spectral CT and will offer perspectives for the future of the field. In particular we will highlight results from micelle and lipoprotein based nanoparticle CT contrast agents.

2 CT image formation

Computed tomography was developed in 1960s and early 1970s by Godfrey Hounsfield and Allan McLeod Cormack.(54) The principle components of a CT scanner are an X-ray source and a detector array. X-rays are emitted from the X-ray source into the patient, where some of them are absorbed. The X-rays that pass through the patient then encounter the detector array, which records the X-ray flux. In one of the more common configurations the source and the detectors rotate around the patient in a synchronized fashion so as to build up a 360 degree dataset where the absorption of X-rays by the patient from all angles is known (Figure 2A). CT images are reconstructed from this dataset by computers using algorithms. Filtered back-projection based reconstruction currently predominates, however, at this current time, iterative and iterative model based reconstruction methods are being introduced.(55)

Early CT scanners had a single row of detectors, and could thus image only a single thin section through the patient known as a slice in one rotation. Volume imaging was performed in a ‘step-and-shoot’ fashion such that a slice was acquired, the patient moved slightly further out of the scanner, another slice acquired and so on. Slices took about 7 minutes to acquire and image reconstruction took hours.(54) Modern scanners have as many as 320 detector rows(56) and scan in what is known as a helical fashion, i.e. the source and the detector constantly rotate and the patient is constantly moved out of the scanner. A 64 detector row scanner can scan 14 cm in under 5 seconds, allowing the entire heart to be imaged in this time.(57) Reconstruction of the set of images takes less than one minute. Images are typically displayed in grayscale, which depends on the attenuation of the different tissues/substances in the field of view (attenuation is the loss of X-ray beam intensity via interactions with matter). More strongly X-ray attenuating substances appear white or light gray, while weakly attenuating substances appear dark gray or black. For example, a CT image of the heart of a patient appears in Figure 2B. The bones, such as the spine on the right of the image, and the contrast agent in the blood pool attenuate X-rays strongly and are light gray. The air, which weakly attenuates X-rays, in front of the patient's chest is black, while tissue, such as the heart muscle, is dark gray. The appearance of the images highly depends on the windowing used, with the maximum and minimum values displayed in the image freely adjustable. Images can also be processed into 3D renderings and displayed in false color such as in Figure 2C. In 2007 it is estimated that there were 10460 CT scanners installed in the USA and 69.5 million CT scans were performed.(58) In 2008, 50.6% of scans were performed on the abdomen, 5.1% for the cardiovascular system, 13.1% for the chest, 24.4% for the brain, 3.4% for the spine and 3.4% for other parts of the anatomy.(59)

3 Principles of CT contrast generation

X-ray attenuation and therefore image contrast results from differential absorption or scattering of the X-rays by tissue. As mentioned above, air absorbs X-rays very weakly,

tissue absorbs X-rays somewhat and bone absorbs X-rays strongly. In the clinic, contrast agents such as iodinated small molecules are injected intravenously to perform angiography, for example, and barium suspensions are used for digestive tract imaging. X-ray absorption and scattering are known together as attenuation, i.e. the reduction of X-ray flux or the number of X-ray photons in the beam. X-ray attenuation in CT is defined on the Hounsfield scale, where the attenuation of any substance is given in Hounsfield Units by the following equation: Attenuation (HU) = $1000*(\mu_x-\mu_{water})/(\mu_{water}-\mu_{air})$

On this scale, the attenuation of air is therefore −1000 HU, that of water is 0 HU, soft tissues range from −100 to 100 HU and bones range from 400 to 1000 HU. Any given element has a characteristic, energy-dependent X-ray attenuation profile, as shown in Figure 3A. Materials attenuate the X-ray beam via two primary mechanisms, the photoelectric effect and the Compton effect.(60) In the photoelectric effect, the photon collides with and transfers its energy to a K-shell electron, typically. The electron is then ejected from its shell and travels a short distance before losing its energy. For a given photon energy, the photoelectric effect scales with Z^3 (Z being atomic number), which can be appreciated in Figure 3A below 33 keV or above 90 keV. This would imply that a high Z element such as gold (Z=79) would create CT contrast 3.3 times greater than that of iodine (Z=53). However, this is not the case. This is because the photoelectric effect is also highly influenced by the energy of the electron shells in the element. If the energy of the X-ray photon is less than that of the electron shell, a photoelectric interaction cannot occur, the X-ray energy must be more than that of the electron shell. The probability of a photoelectric event is maximal at the energy of the electron shell and declines with increasing energy, inversely proportional to the photon energy cubed ($1/E^3$). The energy of the K electron shell for iodine is 33.2 keV, whereas that for gold is at 80.7 keV, resulting in strong attenuation for iodine of X-rays over 33.2 keV in energy, as can be seen in Figure 3A. This feature is known as the K-edge. As many clinical scans are performed at a tube voltage of 80 kV, the K-edge of iodine is strongly influential on its attenuation and greater attenuation advantage of gold from its higher Z value is erased, with approximately equal attenuation from the two elements observed in practice.(61,62)

In the Compton effect, an X-ray photon interacts with a weakly bound electron. The electron absorbs some of the photon energy and the photon moves away from the interaction site in a different direction and with reduced energy, attenuating the beam in the line between the source and the detector. All electrons in low atomic number elements are weakly bound, as are most electrons in high atomic number elements. The primary effect of an element on Compton scattering is, therefore, its density of electrons. As the number of electrons is proportional to atomic mass, electron density and hence Compton related scattering scales with the mass density and is therefore higher for gold (d=19.3 g/cm^3), for example, than it is for water (d=1 g/cm^3).

Air and tissue are composed of elements of similar Z and K-edges (hydrogen, carbon, oxygen and nitrogen), but air is much less dense than tissue, so has very low attenuation, stemming from a low Compton effect. Bone is rich in relatively high Z elements, for organic matter, i.e. calcium and phosphorous (Z=20 and 15, respectively). Therefore the attenuation of bone is high. CT contrast media therefore employ elements that have much higher Z values than those found in the body, such as iodine, barium gold, bismuth and so on. A limitation of CT is its low sensitivity to contrast compared with other imaging techniques. The detection limit for CT is about 10^{-3} M,(61) whereas for MRI it is about 10^{-5} M for gadolinium chelates and for nuclear techniques about 10^{-9} M.(63) This is because for CT, the contrast agent is being directly detected against a high background signal. For MRI, contrast agents increase the signal observed from water in a catalytic fashion, whereas for

nuclear techniques there is no background. This low sensitivity is a major factor in the development of extremely dense, high payload nanoparticles for CT.

It is important to note the characteristics of the X-ray beams sent into the patient in CT imaging. The X-ray tube voltages used range from 80-140 kV. This voltage defines the *maximum* energy of the emitted X-ray photons, however, the beam is composed of a *range* of X-rays, from roughly 25 keV to the maximum energy. For example, typical X-ray spectra emitted when a scanner is run at 80 and 140 kV are depicted in Figure 3B. The X-ray tube generator actually emits X-rays from 0 keV up to the maximum energy, however low energy X-rays are very strongly absorbed in the skin and superficial tissues of the patient and essentially none would reach the detectors, resulting in a needless dose of radiation to the patient. Therefore Teflon or aluminum filters are placed between the X-ray tube generator and the patient which absorb the low energy X-rays and result in the X-ray spectra shown.

The CT contrast that will be generated by an element hence depends on its attenuation characteristics from 25 keV up to the maximum energy. The X-ray attenuation profiles of elements can be accessed freely online from a NIST database(64) and the attenuation profile of several elements are displayed in Figure 3A. Comparisons of, or simulations run on the distribution of the X-ray beam and the attenuation profile will give a reasonable idea of the performance of the contrast agent at different energies. For example, the K-edge of iodine is at 33.2 keV, so iodine gives stronger contrast when scanned at 80 kV than 120 kV, as in the latter case more of the X-rays are in a region of the spectrum where iodine absorbs poorly.(61,62) On the other hand, the K-edge of gold is at 80.7 keV, meaning that it absorbs X-rays strongly in the 80-120 keV region and hence it provides stronger contrast when scanned at 120 kV that at 80 kV. Gold produces about 2.1 times the contrast of iodine when scanned at 120 kV.(61)

Nevertheless, one more important point to note is that the contrast generation properties of an agent are different when scanned in air as compared to in a patient. This is because the tissues and bones of the patient absorb some of the lower energy X-rays in the beam, in a process called beam hardening and therefore the average X-ray energy the contrast agent is exposed to within the patient is increased. To allow an evaluation of a novel CT contrast agent that is relatable to the clinical situation, and to standardize contrast agent comparisons, we recommend the following steps:(61,65)

-Use of clinical scanners, as opposed to micro CT or synchrotron systems.

-Placing the samples in a volume of water that approximately mimics the size and shape of a patient, not to simply scan the samples in air.

-Calculation of a measure termed attenuation rate, which is the attenuation in HU divided by the agent concentration in mM, determined from scanning a range of concentrations.

In view of the energy dependent attenuation exhibited by X-ray contrast media and the development of spectral CT, Hurrell et al. recently proposed a new form of units to measure CT contrast, i.e. spectral Hounsfield units.(66) In these units, the average energy of the X-ray beam (in keV) is denoted with a subscript, e.g. HU_{90}, when the average energy of the beam is 90 keV. We agree in principle with these units and have suggested a modification where the energy range is given as a subscript, e.g. $HU_{25\text{-}140}$. Therefore attenuation rates should be given in spectral Hounsfield units, in the form $HU_{XX\text{-}YY}$/mM.(65)

4 Nanoparticle types and structures

A myriad of different nanoparticle types have been reported for biomedical applications, such as liposomes, emulsions, micelles, lipoproteins, viruses, polymeric nanoparticles, solid metal nanoparticles, silica, metal oxides or other salts, carbon nanotubes, graphene sheets and so forth.(21,25,67-71) For CT the nanoparticles that have been studied are mainly either lipid-based structures (liposomes, emulsion, micelles or lipoproteins),(7,9,46,50,72,73) solid core based (metal, metal alloy or metal salt)(29,32,49) or combinations of the two.(28,44,48) Lipid-based structures are particularly appealing as nanoparticles for biomedical applications due to their ease of synthesis and inclusion of multiple functional substances, as well as their general biocompatibility.(25) A summary of lipid based nanoparticle types is shown in Figure 4. A liposome is an aggregate of lipids formed into a bilayer that encloses an aqueous core. Functional cargoes can be loaded in the core or in the lipid layer of this nanoparticle. An emulsion is a tiny droplet of a hydrophobic substance, such as oil, that is encapsulated in a lipid coating. Emulsions can be loaded with cargoes in the hydrophobic core, the lipid layer, or the core itself may be functional.

Micelles are closed lipid monolayers with a hydrophobic fatty acid core and hydrophilic polar surface. Lipids in solution assemble into micelles when their concentration exceeds the critical micelle concentration (CMC) of the lipid in question. The difference between lipids that form micelles and lipids that form liposomes lies in the relative sizes of their hydrophobic tails and hydrophilic headgroups. If the headgroup is much wider than the tail then the molecule will have a cone-like shape and will form a micelle. On the other hand, if the headgroup and the tail are similar in width then the shape will be cylindrical and liposome formation will be favored. For example, phospholipids with a small tail, such as a single hydrocarbon chain are more likely to form micelles, whereas phospholipids with two hydrocarbon chains are more likely to form liposomes.(74) Lipoproteins, particularly high-density lipoprotein (HDL), are natural nanoparticles that transport cholesterol within the bloodstream.(75) They can be considered to be a form of micelle, being composed of a single lipid layer, into which is embedded amphipathic proteins, and with a hydrophobic core.(69) Both micelles and lipoproteins have been studied as drug/gene delivery platforms(76-79) as well as contrast agents or tracers for MRI, PET and fluorescence.(25,80) Micelles and lipoproteins can be made functional as CT contrast agents by either forming them from lipids that contain contrast generating atoms, such as iodine,(46) or by encapsulating hydrophobically coated metal/metal salt cores, such as gold or bismuth sulfide.(28,48) In the following sections we will review the different types of nanoparticles that have been used as CT contrast agents and will highlight micelle-based nanoparticles in particular.

5 Non-targeted nanoparticles for CT imaging

5.1 Iodine-based agents

The first nanoparticles reported for CT imaging were iodine-based, being based on clinically approved small molecule agents.(7,81) These nanoparticles were primarily emulsions of ethiodized oil or liposomes that encapsulate iodinated small molecules.(6,8,82-84) Vermess et al. reported emulsions of ethiodized poppy seed oil (Ethiodol) as early as 1979.(8) These particles were formed by homogenization of the oil with lipids such as Tween or lecithin, resulting in structures such as IV in Figure 4. These particles were in the 1-5 micron size range, so too large to be nanoparticles. The agent was rapidly taken up by the liver. It was translated to the clinic, where efficacy for liver tumor imaging was observed,(6) but further development was halted because of side effects caused by macrophage activation that were not acceptable for a diagnostic agent. This work, however, laid the foundation for the development of subsequent nanoparticle formulations(6,82) and, in fact, several recently

reported formulations are based on the same technology, albeit synthesized with refined techniques and improved lipid coatings.(85-89) For example, Bakan et al. used microfluidic processing and dioleoylphosphatidylcholine (DOPC) to create emulsions from polyiodinated triglycerides 200-300 nm in diameter.(82) Inclusion of cholesterol in a 0.4:1 cholesterol:DOPC ratio resulted in a markedly more stable formulation than without cholesterol. A more extensive discussion of these older formulations can be found in a review article by Krause.(11)

In 2013, Ding et al. reported an emulsion of iodinated oil with polyethylene glycol (PEG) monostearate as the lipid.(87) Hydrophobically coated quantum dots were included in the oil core to provide fluorescence contrast. The emulsions could be concentrated to 240 mg I/ml and produced intense CT contrast. These nanoparticles were shown to be taken up by macrophages in vitro and to accumulate in the plaques of atherosclerotic rabbits at 2 hours post-injection by CT and fluorescence imaging. De Vries et al. reported nanoemulsions of small size (>100 nm) formed from triiodo-benzene alkyl ester oils.(85) These nanoemulsions were synthesized by emulsification of the oils with either PEGylated phospholipids or block co-polymer amphiphiles via the use of a microfluidizer. The smallest and most stable formulations were used in vivo. Marked contrast (up to 190 HU) was observed in the heart and blood vessels immediately after injection. Contrast was also observed in the liver and spleen, but had dissipated after one week, indicating extensive excretion. Nanoemulsion circulation half-lives of up to 2.7 hours were found. Asides from experimental formulations, a nanoemulsion loaded with iodinated oil is commercially available for preclinical experiments.(90)

Liposomes encapsulating clinically approved iodinated contrast media have been studied since the 1980s.(91-93) As mentioned above, liposomes consist of a lipid bilayer that contains an aqueous core. This aqueous core typically contains a payload such as a drug or contrast agent – one of the first clinically approved nanoparticles was Doxil, a liposomal formulation of doxorubicin.(17) The advantage of using liposomes for CT is that it is relatively easy to synthesize them from clinically approved components, i.e. lipid mixtures and clinically approved iodinated contrast media, although it is challenging to achieve high iodine payloads/concentrations. Such formulations yield long lasting CT contrast(50) and, it is theorized, may prove compatible with patients whose kidney function is poor due to slow release of the encapsulated payload. In fact, a company(94) is currently developing a liposomal CT contrast agent and aims to start clinical trials within the next two years.(95) Such liposomes are typically formed by hydration of either a lipid film or an organic solution of lipids with an aqueous solution that contains an iodinated contrast agent.(50,92) Additional processing such as extrusion using ~200 nm pore size membranes results in small, unilamellar liposomes with a narrow size distribution.(50) The unencapsulated contrast agent is removed by dialysis and the formulation is concentrated. Likely due to poor pharmacokinetics, some of the older liposomal formulations were not reported to be blood pool agents, but were observed to accumulate in the liver and spleen.(91) Liver tumors could be visualized as darker regions, due to poor accumulation of the liposomes in the tumors compared with the liver. Later formulations saw the introduction of PEGylated surfactants to the lipid mixture, which resulted in longer blood circulation times.(84) Recent developments include liposomes that co-encapsulate both iodinated and gadolinium-chelating molecules, providing MRI and CT contrast.(96) Furthermore, Miyata et al. reported a liposome that co-encapsulated sodium borocaptate and an iodinated contrast agent.(97) The purpose of the sodium borocaptate was to facilitate boron neutron capture therapy, so the liposome has both diagnostic and therapeutic functions, otherwise known as theranostics. The liposome was targeted with transferrin, whose receptor is overexpressed in certain cancers such as gliomas. The targeted liposomes were found to accumulate in glioma tumors in the brains of rats to a greater extent (82.2 vs. 22.5 μg B/g) than non-targeted liposomes. The advantage of

CT imaging of the liposome distribution is that it would allow more effective planning of neutron therapy.

An alternative approach to develop lipid structures that produce contrast for CT has been to synthesize them from lipids that are themselves labeled with iodine or other contrast generating elements. One of the first examples of this was published by Caride et al., where brominated phospholipids were formed into liposomes and administered to dogs.(30) Contrast enhancement of up to 40 HU was observed in the liver and spleen. Notably, the Torchilin group has developed polymeric, iodinated micelles as CT contrast agents.(98) A 12 kDa hydrophilic PEG chain was conjugated to a 12-repeat unit polylysine polymer. The free amine groups of the polymer were reacted with 2,4,6-triiodobenzoic acid to synthesize an iodinated lipid, which was used to form micelles (Figure 5A, B).(47) The iodine content of the micelles was 17.7% by weight. Rats were scanned using CT at 80 kV before and after injection with such micelles at a dose of 170 mg of iodine per kg. As can be seen in Figure 5C, at two hours post-injection, strong contrast (150 HU) could still be observed in the heart, and with contrast in the liver and spleen of 57 and 90 HU respectively.(46) This agent is clearly effective for providing long-lasting blood pool contrast and also liver and spleen imaging. More recently, the group of Conyers has developed liposomes composed of lipids that contain iodine, as potential CT contrast agents.(99)

Dendrimers are branched polymer molecules that are frequently used as scaffolds to develop into contrast agents. One of the most often used dendrimer types is poly(amidoamine) or PAMAM, which possesses multiple amine groups, allowing easy modification with a variety of functionalities. The Brechbiel group first proposed iodinated dendrimers as CT contrast agents.(27) They reacted a triiodobenzenepropanoic acid derivative with a PAMAM dendrimer to create an agent that was 33% iodine by mass. The agent was shown to produce CT attenuation.(100) Fu et al. reported several PEG-core, polylysine dendrimers that had been coupled with a clinically approved contrast agent, iobitridol.(101) The physicochemical properties, such as solubility, hydrophilicity, viscosity and osmolality were carefully evaluated. While the solubility was over 440 mg of iodine/ml and the dendrimers were very hydrophilic, unfortunately the viscosity and osmolality were higher than commercial agents, when adjusted for concentration.(101) Strong contrast was observed in the blood vessels of rats at 2 minutes post-injection of one of these dendrimers. While the contrast produced was longer lasting than that of small molecule agents, it had largely dissipated after 32 minutes.

One of the attractive features of dendrimers is the ease of adding additional contrast generating groups. For example, Guo et al. synthesized dendrimers that entrapped gold nanoparticles and subsequently reacted them with diatrizoic acid.(102) This double labeling resulted in enhanced contrast as compared with dendrimers labeled with gold nanoparticles alone. To create a dual modality contrast agent, Criscione et al. labeled dendrimers with both triiodobenzoic acid and technicium, providing contrast for single photon emission tomography as well as CT.(103)

5.2 Gold-based agents

Gold nanoparticles have been proposed for a myriad of biomedical applications,(104) such as photoacoustic imaging, photothermal ablation and DNA detection, to name but a few.(19,105,106) Synthetic approaches to gold nanoparticles are well developed, in terms of control over their size, morphology and surface chemistry.(107-110) They are generally regarded as biocompatible(111) and are undergoing evaluation as therapeutic agents in a number of clinical trials.(43,112-114) In a 2006 publication Hainfeld reported a 1.9 nm gold nanoparticle formulation as a contrast agent for X-ray imaging.(115) Rats were injected with these nanoparticles at a dose of 2.7 g of gold/kg. Comparison of pre- and two minutes post-

injection X-ray images revealed that the agent strongly opacified the blood vessels of the rats, although such a high dose would likely not be economical to use in practice. Images acquired at subsequent timepoints showed the agent to be excreted via the kidneys and the urine over approximately an hour. No toxicity was observed from hematology, blood chemistry or histology.

Encouraged by these results, two groups investigated large, long circulating gold nanoparticles as CT contrast agents, both publishing their results in 2007.(26,49) Cai et al. synthesized 10 nm core diameter gold nanoparticles coated with PEG-2000, resulting in a hydrodynamic diameter of 38 nm.(49) In vitro experiments, as well as observations, hematology, blood chemistry or histology again showed no signs of toxicity, although transmission electron microscopy and inductively coupled plasma mass spectrometry measurements showed extensive liver retention at three days post-injection. From experiments with mice at a dose of 493 mg of gold/kg, the circulation half-life was found to be 14.6 hours and contrast of over 100 HU was seen in the aorta for up to 24 hours. Thus this agent provided excellent blood pool contrast, which allowed tumor neovasculature to be resolved.(49) The difference in the excretion between this agent and the one reported by Hainfeld is due to the nanoparticle diameter. It is thought that small, sub-5 nm nanoparticles can be swiftly excreted by the kidneys, whereas larger nanoparticles are too big to pass through the kidney and are retained in the bloodstream.(116) A number of other gold nanoparticle platforms have been developed, using stabilizers such as dendrimers,(117-120) thioctic acid,(121) gum Arabic(122,123), PLGA(124) or heparin.(125)

Several groups have pursued multifunctional gold nanoparticles, i.e. formulations that have an additional diagnostic or therapeutic functionality. In an interesting example, von Maltzahn et al. used gold nanorods as CT contrast agents and for photothermal tumor therapy.(19) 13 by 47 nm PEGylated gold nanorods were injected into mice bearing tumors. CT imaging was used to visualize the accumulation of the gold nanorods in the tumors and plan the laser irradiation needed for treatment. The gold nanorods used absorb light strongly in the near-infrared (NIR) window, a region of the electromagnetic spectrum where tissue absorbs weakly. The absorption of light results in localized heating and cell death. Such treatment of the mice bearing tumors resulted in elimination of the tumor and survival of the mice over a 50 day period.(19)

Gadolinium containing chelates can be added to gold nanoparticle surfaces to produce a contrast agent active for both CT and MRI.(28,41,126-128) The first example of this type of nanoparticle was published by Alric et al. A diethylene triamine pentaacetic acid (DTPA) chelate molecule functionalized with thiol groups was used as a capping ligand during the synthesis of the gold nanoparticles. Complexation with gadolinium ions resulted in the final product. CT and MRI phantom imaging demonstrated the contrast generating properties of this nanoparticle. Sun et al. formed CT/MRI active gold nanorods in a micelle-based approach.(128) The authors prepared gold nanorods with a hydrophobic, dodecanethiol coating. These nanorods were encapsulated in the core of micelles formed from lipids whose headgroup was a gadolinium-DTPA chelate. The contrast generating potential of the nanorods was demonstrated via CT and MRI phantom imaging. Although not demonstrated in the paper, the rods should also provide fluorescent contrast.(129)

Van Schooneveld et al. reported a trimodality, micelle-based gold nanoparticle contrast agent for CT, MRI and fluorescence contrast.(28) 66 nm gold nanoparticles were synthesized and then coated with an 11 nm layer of silica. These nanoparticles were made hydrophobic by absorption of octadecanol on the surface. The resulting nanoparticles were then suspended in the core of micelles composed of a mixture of lipids (Figure 6A,B). The lipid headgroups contained Gd-DTPA, PEG or the NIR fluorophore Cy5.5. The contrast

generating potential of these nanoparticles was demonstrated via phantom imaging and by imaging macrophage cells that had been incubated with the nanoparticles. Furthermore, mice were scanned before and 24 hours after injection with these nanoparticles with CT and MRI (Figure 6C,D). Contrast was observed in the livers of these animals post-injection. Last, the livers of mice injected with fluorescent and non-fluorescent micelles gold nanoparticles were imaged; contrast could also be clearly observed (Figure 6E).

5.3 Bismuth-based agents

Bismuth is also an appealing element upon which to base CT contrast agents. It has a similar Z to gold and also produces contrast that varies little with X-ray tube voltage.(130) It is regarded as being one of the most biocompatible of the heavy elements, although its ionic form is toxic at 0.2 M,(131) and it is much cheaper than gold. However, compared to gold nanoparticles, there is much less known about their synthesis, in terms of control over size, shape and surface chemistry. Additionally, bismuth is half as dense as gold and synthesizing elemental bismuth nanoparticles is challenging;(132) other ions such as sulfur are frequently needed.(29,40,48,133,134) Both these factors mean that bismuth nanoparticles typically have a lower payload than comparable gold nanoparticles.

Rabin et al. were the first to report bismuth nanoparticles as CT contrast agents.(29) The authors formed bismuth sulfide nanoparticles from co-precipitation of bismuth citrate and sodium sulfide in the presence of 3-mercaptopropionic acid, which acted as a surfactant. The nanoparticles were further coated with polyvinylpyrrolidone (PVP). This resulted in plate-shaped nanoparticles. In cytotoxicity assays, no effect on the viability of macrophages or hepatocytes was observed below 20 mM Bi, but reductions of viability were observed at concentrations above 20 mM. CT imaging experiments performed in mice revealed the agent to perform well as a blood pool agent, with a maximum enhancement of 557 HU and a blood half-life of 140 minutes, when injected at a dose of 477 mg Bi/kg. Furthermore, subcutaneous injections of the agent drained into the lymph nodes, which could be visualized with CT, hence demonstrating potential for lymph node imaging.

Several other approaches for synthesizing bismuth nanoparticles as CT contrast agents have been reported. Perera et al. synthesized PVP coated nanoparticles composed of a bismuth-iron inorganic coordination polymer, although the use of cyanide brings into question their biocompatibility.(134) A large-scale synthesis of Bi_2S_3 nanoparticles was reported by Ai et al.(133) Thioacetamide dissolved in oleylamine was injected into a solution of hot bismuth neodecanoate in octadecene, producing the nanoparticles in a thermal decomposition reaction. Again, PVP was used to coat the nanoparticles. The resulting cores were 2-3 nm in diameter, however, the nanoparticles were observed to accumulate in the livers of rats in CT images. Elemental bismuth nanoparticles have been synthesized by Brown et al., via the reduction of bismuth nitrate with sodium borohydride in the presence of dextran.(132) This resulted in bismuth cores of 19.5 nm diameter on average and 130 nm hydrodynamic diameter due to the coating. Interestingly, Andreś-Vergeś et al. reported a co-precipitation of bismuth nitrate and iron (II) sulfate to form iron oxide nanoparticles with a bismuth oxide shell.(135) Due to the iron oxide core, these nanoparticles have the potential for combined CT and MR imaging.

5.4 Agents based on other elements

As mentioned above, some of the first nanoparticles developed as CT contrast agents were based on bromine, such as liposomes formed from brominated phospholipids.(30) Furthermore, nanoemulsions of perfluorooctylbromide were extensively studied as contrast agents for CT, as well as MRI and ultrasound, in the 1980s and 1990s.(12,73,136) Perfluorooctylbromide is an eight carbon chain with one bromine substituent and the other

substituents being fluorine. It is highly biocompatible, with no adverse responses observed in dogs at an injected dose of 1g/kg or in humans with an oral dose of up to 12 ml/kg.(73) Emulsions of perfluorooctylbromide formed with lecithin were found to be effective as both blood pool and liver imaging agents.(137) Liver imaging allowed identification of tumors and abcesses.(10,138) Furthermore, this agent was found to be effective for detecting liver tumors with CT in clinical trials.(12) However, the agent did not progress due to flu-like symptoms caused by macrophage activation.(12) Furthermore, bromine is limited by the relatively weak contrast it produces and its low loading density (only one bromine atom per perfluorooctylbromide molecule).

A variety of other elements have been used to form nanoparticle CT contrast agents, such as platinum,(32) gadolinium,(34,139) ytterbium,(140) yttrium(34) and tantalum,(31,141-143) although there are concerns over the use of gadolinium, due to its potential for toxicity.(144) Nevertheless, gadolinium has been used to create some interesting, multifunctional nanoparticles that produce contrast for CT, MRI and fluorescence.(34,139) The recent work on tantalum nanoparticles is of particular interest as most of the publications come from a focused effort by General Electric employees, indicating a substantial investment from industry. These nanoparticles have been characterized for their CT contrast properties, their in vivo imaging efficacy, pharmacokinetics, biodistribution and their physiochemical properties.(141-143) Furthermore, large scale syntheses (up to 500 g) of these nanoparticles have been devised.(142) Tantalum is a relatively cheap and abundant element and the company hopes to put a formulation into clinical trials.(145)

6 Nanoparticles for CT cell tracking

Cell tracking is the process of imaging the delivery and movements of cells in vivo. This is frequently achieved by labeling cells ex vivo, injecting them into the subject and using an imaging technique to track the cells over time. This was first pursued using nuclear imaging in combination with indium-111 labeling.(146) Cell tracking has been extensively pursued for MRI by loading cells with iron oxides and has been used to study stem cell therapies and monocyte behavior, for example.(147-149) This topic has barely begun to be explored for CT. The Bulte group has published several reports on tracking pancreatic islet cells that are encapsulated in alginate.(150) These capsules may be made inherently radiopaque by using barium or bismuth ions to cross-link the alginate, and CT imaging has been used to track such capsules.(151) This group has also explored loading the alginate capsules with the gadolinium labeled gold nanoparticles developed by Alric et al., which were mentioned above.(51) These capsules can be detected with CT, T_1-weighted MRI and ultrasound and co-encapsulation of the cells with the nanoparticles had no effect on the cell viability (CT resolution 83 μm). Furthermore, perfluorooctylbromide nanoemulsions have also been included in these capsules, allowing their detection by CT, ^{19}F MRI and ultrasound.(152) The resolution of the in vivo imaging experiments in this study was 353 μm. Menk et al. used gold nanoparticles coated with horse serum proteins to label cancer cells.(153) These cells were injected into brains of rats and their distribution was imaged with small animal CT systems (30 μm resolution). The application of CT to cell tracking is in its infancy, and progress will likely be challenging due to the poor sensitivity of CT and toleration by the cells of very high levels of contrast media loading. Nevertheless, we anticipate more reports on this topic in the coming years.

7 Targeted nanoparticles for CT imaging

Targeted imaging with CT represents a particular challenge due to its low sensitivity to contrast media. Krause defined the minimum detectable signal change in CT to be 30 HU.(11) With the attenuation rate of gold being 5.1 $HU_{25\text{-}120}$/mM,(61) this implies that the

minimum detectable concentration difference between target and background is 5.9 mM. Despite the varying contrast generating properties of CT contrast media, the required concentration of any other agent will be reasonably close to this value. Accumulating such concentrations of contrast media at target sites is difficult. Nevertheless, using nanoparticles densely loaded with CT contrast media and applying them to highly expressed targets, targeted imaging with CT has been shown to be feasible.(154) Furthermore, in certain clinical settings, such as imaging atherosclerosis in the coronary arteries, CT is preferable to alternative imaging methods (MRI, PET). So developing molecular imaging of atherosclerosis for CT, for example, would be highly attractive.

Consequently, the first targeted CT contrast agent was reported for imaging thrombi, whose occurrence in the arteries is the source of heart attacks, strokes and other adverse cardiovascular events. Thrombi are mostly composed of densely packed fibrin, enabling their detection with CT via fibrin targeting. Nanoemulsions loaded with either perfluorooctylbromide or an iodinated oil were synthesized and modified to have an anti-fibrin antibody attached to their surface.(154) Clots were formed from human plasma in vitro and were incubated with the targeted nanoparticles. Strong attenuation was observed in the clots in vitro. The targeting was proven by a competitive-inhibition experiment where incubation with an excess of free anti-fibrin antibodies caused a five-fold decrease in the contrast to noise ratio in the clot. Subsequently the same group reported nanoparticles loaded with either Ethiodol oil or bismuth neodecanoate complexes, with a cross-linked block co-polymer coating.(155) A similar anti-fibrin targeting strategy was pursued to perform in vitro imaging of clots.

An example of a micelle-based targeted nanoparticle was reported by Kinsella et al.(48) Bismuth sulfide nanoparticles were synthesized via the addition of a solution of elemental sulfur to bismuth acetate and oleic acid in boiling octadecene. This resulted in hydrophobically coated (oleic acid), 10 nm core nanoparticles. These nanoparticles were made biocompatible by mixing with PEG-phospholipids and forming a lipid film, which was hydrated with PBS. Some of the PEG-phospholipids used were functionalized with maleimide and amines at the distal end, which were used to attach the LyP-1 peptide or the NIR fluorophore Cy7, respectively (Figure 7A). The LyP-1 peptide was developed in a phage display methodology to preferentially target breast cancer cells.(156) In vitro assays and biodistribution analysis showed that the targeted nanoparticles were more extensively taken up in cancer cells than non-targeted nanoparticles (Figure 7B). Comparison of CT images acquired immediately after and 24 hours post-injection of LyP-1 targeted nanoparticles revealed significant contrast in tumors (Figure 7C,D).

As mentioned above, lipoproteins can be considered to be a form of micelle. Cormode et al. reported a gold core high-density lipoprotein nanoparticle that was targeted to macrophages in atherosclerotic plaque, and whose accumulation in the aorta of a mouse model could be detected with microCT imaging.(45) Hyafil et al. also targeted macrophages with an iodinated polymeric nanoparticle.(157) These experiments were carried out in a rabbit model of atherosclerosis using clinical CT scanners.

Several other groups have published studies about nanoparticle CT contrast agents targeted to cancer. In 2008, Popovtzer et al. reported gold nanorods that had been conjugated with anti-antigen A9, which is over expressed in squamous cell carcinoma.(158) Image analysis results from CT images of cell pellets indicated the targeting to be successful. The Montet group targeted iodine loaded liposomes with E-selectin specific peptides.(159) E-selectin is overexpressed in tumor vasculature, so injections of this targeted formulation resulted in enhanced and E-selectin specific accumulation in tumor bearing mice. Hill et al. developed a low-density lipoprotein (LDL) like nanoparticle loaded with iodinated triglycerides that was

shown to be taken up in HepG2 cancer cells, which over express the LDL receptor.(72) Platinum-iron alloy nanoparticles were targeted with antibodies to the Her2 receptor.(32) In vitro experiments showed this nanoparticle to be preferentially taken up by cancer cells that over expressed the Her2 receptor. Eck et al. conjugated antibodies against the CD4 receptor to 38 nm gold nanoparticles.(160) CT imaging showed these nanoparticles to preferentially accumulate in the lymph nodes when compared with IgG targeted control nanoparticles.

8 Nanoparticles used with spectral CT

In 2008 Schlomka et al. reported the development of a new type of CT scanner, called spectral or multicolor CT, by Philips.(52) This prototype scanner can distinguish different materials in the field of view, such as gold, iodine, bismuth, ytterbium, gadolinium, calcified tissue and soft tissue, displaying the distributions of these materials in different colors, hence the name multicolor CT.(33,40,44,161) The primary difference between this scanner and a conventional CT scanner lies in the detectors.(52,162-164) The spectral CT scanner has detectors whose sensor material is cadmium telluride, allowing the detection of the energy of incident X-rays. When an X-ray hits this kind of detector, a current pulse is generated. The magnitude of the current is proportional to the X-ray energy, and each current pulse occurrence is recorded in one of several data channels, depending on its magnitude. The bounds of the channels are freely adjustable and can be altered to match the K-edges of the contrast agents used in each experiment. For example, we have used 25–34, 34–51, 51–80, 80–91, 91–110, and 110–130 keV when imaging iodine and gold based contrast agents in the same experiment. The first and third energy boundaries match the K-edges of iodine and gold, respectively, to facilitate detection of these elements. Calculations performed on the six data sets produced allow the spatial distribution and concentration of the materials in the field of view to be determined and rendered as images.(165,166)

We have employed spectral CT in conjunction with nanoparticles in a mouse model of atherosclerosis.(44) In coronary imaging with conventional CT, iodinated clinical contrast agents are used to delineate areas of luminal narrowing, or stenoses, which may require stent emplacement.(167) In addition, detection of calcium deposits, otherwise known as calcium scoring, is another important method to estimate the cardiovascular risk of a patient.(168) Last, as mentioned before, macrophage content of atherosclerotic plaque has been established as a marker for vulnerability to rupture.(169) In this study we used a gold nanoparticle, whose coating is similar to that of high-density lipoprotein, which we had previously shown to be specific for macrophages in atherosclerosis (Figure 8A,B).(45) Therefore we attempted to use spectral CT to characterize three parameters of atherosclerotic plaque simultaneously, i.e. stenosis, calcification and macrophage content.

Phantom imaging proved that spectral CT could distinguish iodine, gold and calcified material in the same field of view (Figure 8C). The gold nanoparticles were injected into atherosclerotic mice. After 24 hours the same mice were injected with a long circulating iodine nanoparticle contrast agent. The mice were imaged with the spectral CT system. As can be seen in Figure 8D, the lumen of the mouse aorta is highlighted with the iodine agent and a nearby macrophage-rich plaque has taken up gold nanoparticles. While no calcifications were observed in the plaque of these mice, the bones are clearly detected, indicating that calcifications, if present, could be identified by the system.

Pan et al have used thrombus targeted bismuth nanoparticles together with spectral CT.(40) Thrombi form in arteries when atherosclerotic plaque ruptures and smaller thrombi are also a marker for unstable plaque, hence imaging them is of great interest in cardiovascular disease. These bismuth nanoparticles are formed from a bismuth fatty-acid complex in a sorbitan sesquioleate matrix that was coated with phospholipids to provide biocompatibility.

Biotin phospholipids included in the coating and incubation with avidin tagged fibrin-specific antibodies resulted in thrombus targeted bismuth nanoparticles. Incubation of these nanoparticles with clots in vitro and as well as clots formed in the iliac arteries of rabbits, resulted in accumulations of the nanoparticles in the clots which were detectable by the spectral CT scanner. The same group has recently reported an ytterbium-based nanoparticle which was targeted to thrombi in the same fashion.(33) The benefit of using ytterbium based nanoparticles is that the sensitivity of their detection is higher than for bismuth, due to a greater discontinuity in attenuation at the K-edge.(170)

9 Summary and Outlook

As we have described above, there has been tremendous progress in nanoparticle contrast agents for CT in the past decade. Improved blood pool agents have been developed, new elements have been introduced (gold, bismuth, tantalum, etc), targeted and cell tracking agents have been reported and specific detection with spectral CT is now possible. Several advanced blood pool agents, such as long-circulating iodine loaded liposomes and small, renally excretable gold or tantalum oxide nanoparticles are nearing clinical trials.(50,115,142) These formulations may benefit patients with compromised renal function, as well as patients with hypersensitivity to iodine contrast agents. Furthermore, their different pharmacokinetic properties to small molecule agents may allow imaging over a wider time window and improved perfusion imaging. The developments in CT technology, such as dual energy CT or spectral CT, that allow specific detection of contrast media are highly beneficial.

Despite this positive outlook, a number of additional areas need to be addressed. Further progress in synthetic approaches is needed to develop cheap, high contrast density nanoparticles that can be synthesized on a large scale. Targeted agents need to be further validated in additional animal models and be studied and optimized for their physicochemical properties. Evaluation of CT contrast properties should be standardized.(61) The field would benefit from greater interactions between the chemists developing novel agents and the radiologists and other clinicians who may eventually use them. Last, the use of contrast agents for CT entails the use of large quantities of heavy elements, which will always pose a risk of toxicity. Thorough toxicological evaluations will be needed to assess the issue of side effects that prevented clinical translation of nanoparticles in the 1980s.(12) Nevertheless, the field has seen rapid advancement in the past decade and we expect to see similar progress made in the coming decade.

Acknowledgments

This work was supported by the National Heart, Lung, and Blood Institute, National Institutes of Health, as a Program of Excellence in Nanotechnology (PEN) Award, Contract #HHSN268201000045C, as well as by R01 EB009638 (Z.A.F.) and R00 EB012165 (D.P.C.).

References

1. Yu S-B, Watson AD. Metal-based X-ray contrast media. Chem Rev. 1999; 99:2353–2377. [PubMed: 11749484]
2. Rumberger JA. Coronary computed tomography angiography. J Am Coll Cardiol. 2008; 52(21): 1733–1735. [PubMed: 19007694]
3. Lumbroso P, Dick CE. X-ray attenuation properties of radiographic contrast media. Med Phys. 1987; 14:752–758. [PubMed: 3683304]
4. Yu S-B, Droege M, Segal B, Kim S-H, Sanderson T, Watson AD. Cuboidal W3S4 cluster complexes as new generation X-ray contrast agents. Inorg Chem. 2000; 39(6):1325–1328. [PubMed: 12526428]

5. Engelbrecht V, Koch JA, Rassek M, Modder U. Gadodiamid und Gadolinium-DTPA als intravenöse Kontrastmittel in der Computertomographie [Gadolinium-DTPA and gadodiamide as an alternative contrast medium for CT]. Rofo. 1996; 165:24–28. [PubMed: 8765359]
6. Sugarbaker PH, Vermess M, Doppman JL, Miller DL, Simon R. Improved detection of focal lesions with computerized tomographic examination of the liver using ethiodized oil emulaion (EOE-13) liver contrast. Cancer. 1984; 54:1489–1495. [PubMed: 6089990]
7. Violante MR, Dean PB, Fischer HW, Mahoney JA. Particulate contrast media for computed tomographic scanning of the liver. Investigative Radiol. 1980; 15(6 Suppl):S171–S175.
8. Vermess M, Chatterji DC, Doppman JL, Grimes G, Adamson RH. Development and experimental evaluation of a contrast medium for computed tomographic examination of the liver and spleen. J Comput Assist Tomo. 1979; 3(1):25–31.
9. Longino MA, Weichert JP, Schwendner SW, Szabo SM, Counsell RE, Glazer GM. Biodistribution of a new lipid-soluble CT contrast agent. Evaluation of cholesteryl iopanoate in the rabbit. Investigative Radiol. 1983; 18(3):275–278.
10. Mattrey RF, Long DM, Multer F, Mitten R, Higgins CB. Perfluoroctylbromide - a reticuloendothelial-specific and tumor-imaging agent for computed-tomography. Radiology. 1982; 145(3):755–758. [PubMed: 7146408]
11. Krause W. Delivery of diagnostic agents in computed tomography. Adv Drug Deliv Rev. 1999; 37:159–173. [PubMed: 10837733]
12. Behan M, O'Connell D, Mattrey RF, Carney DN. Perfluorooctylbromide as a contrast agent for CT and sonography - preliminary clinical-results. Am J Roentgenol. 1993; 160(2):399–405. [PubMed: 8424361]
13. Jana NR, Gearheart L, Murphy CJ. Wet chemical synthesis of high aspect ratio cylindrical gold nanorods. J Phys Chem B. 2001; 105(19):4065–4067.
14. Nehl CL, Liao H, Hafner JH. Optical properties of star-shaped gold nanoparticles. Nano Lett. 2006; 6(4):683–688. [PubMed: 16608264]
15. Song KH, Kim C, Cobley CM, Xia Y, Wang LV. Near-infrared gold nanocages as a new class of tracers for photoacoustic sentinel lymph node mapping on a rat model. Nano Lett. 2009; 9:183–188. [PubMed: 19072058]
16. Kim BYS, Rutka JT, Chan WCW. Nanomedicine. N Eng J Med. 2010; 363(25):2434–2443.
17. Peer D, Karp JM, Hong S, Farokhzad OC, Margalit R, Langer R. Nanocarriers as an emerging platform for cancer therapy. Nat Nanotech. 2007; 2:751–760.
18. Frank-Kamenetsky M, Grefhorst A, Anderson NN, Racie TS, Bramlage B, Akinc A, Butler D, Charisse K, Dorkin R, Fan Y, Gamba-Vitalo C, Hadwiger P, Jayaraman M, John M, Jayaprakash KN, Maier M, Nechev L, Rajeev KG, Read T, Rohl I, Soutschek J, Tan P, Wong J, Wang G, Zimmermann T, de Fougerolles A, Vornlocher HP, Langer R, Anderson DG, Manoharan M, Koteliansky V, Horton JD, Fitzgerald K. Therapeutic RNAi targeting PCSK9 acutely lowers plasma cholesterol in rodents and LDL cholesterol in nonhuman primates. Proc Natl Acad Sci USA. 2008; 105(33):11915–11920. [PubMed: 18695239]
19. von Maltzahn G, Park JH, Agrawal A, Bandaru NK, Das SK, Sailor MJ, Bhatia SN. Computationally guided photothermal tumor therapy using long-circulating gold nanorod antennas. Cancer Res. 2009; 69(9):3892–3900. [PubMed: 19366797]
20. Corot C, Robert P, Idee J-M, Port M. Recent advances in iron oxide nanocrystal technology for medical imaging. Adv Drug Deliv Rev. 2006; 58:1471–1504. [PubMed: 17116343]
21. Cormode DP, Skajaa T, Fayad ZA, Mulder WJM. Nanotechnology in medical imaging: probe design and applications. Arterioscler Thromb Vasc Biol. 2009; 29:992–1000. [PubMed: 19057023]
22. Medintz IL, Uyeda HT, Goldman ER, Mattoussi H. Quantum dot bioconjugates for imaging, labelling and sensing. Nat Mater. 2005; 4:435–446. [PubMed: 15928695]
23. Moghimi SM, Hunter AC, Murray JC. Long-circulating and target-specific nanoparticles: Theory to practice. Pharmacol Rev. 2001; 53:283–318. [PubMed: 11356986]
24. Mulder WJM, Griffioen AW, Strijkers GJ, Cormode DP, Nicolay K, Fayad ZA. Magnetic and fluorescent nanoparticles for multimodality imaging. Nanomedicine. 2007; 2(3):307–324. [PubMed: 17716176]

25. Mulder WJM, Strijkers GJ, Van Tilborg GAF, Cormode DP, Fayad ZA, Nicolay K. Nanoparticulate assemblies of amphiphiles and diagnostically active materials for multimodality imaging. Acc Chem Res. 2009; 42(7):904–914. [PubMed: 19435319]
26. Kim D, Park S, Lee JH, Jeong YY, Jon S. Antibiofouling polymer-coated gold nanoparticles as a contrast agent for in vivo x-ray computed tomography imaging. J Am Chem Soc. 2007; 129(24): 7661–7665. [PubMed: 17530850]
27. Yordanov AT, Lodder AL, Woller EK, Cloninger MJ, Patronas N, Milenic D, Brechbiel MW. Novel iodinated dendritic nanoparticles for computed tomography (CT) imaging. Nano Lett. 2002; 2(6):595–599.
28. van Schooneveld MM, Cormode DP, Koole R, van Wijngaarden JT, Calcagno C, Skajaa T, Hilhorst J, Hart DC, Fayad ZA, Mulder WJM, Meijerink A. A fluorescent, paramagnetic and PEGylated gold/silica nanoparticle for MRI, CT and fluorescence imaging. Contrast Media Mol Imaging. 2010; 5(4):231–236. [PubMed: 20812290]
29. Rabin O, Perez JM, Grimm J, Wojtkiewicz G, Weissleder R. An X-ray computed tomography imaging agent based on long-circulating bismuth sulphide nanoparticles. Nat Mater. 2006; 5:118–122. [PubMed: 16444262]
30. Caride VJ, Sostman HD, Twickler J, Zacharis H, Orphanoudakis SC, Jaffe CC. Brominated radiopaque liposomes: contrast agent for computed tomography of liver and spleen a preliminary report. Invest Radiol. 1982; 17:381–385. [PubMed: 7129819]
31. Oh MH, Lee N, Kim H, Park SP, Piao Y, Lee J, Jun SW, Moon WK, Choi SH, Hyeon T. Large-scale synthesis of bioinert tantalum oxide nanoparticles for x-ray computed tomography imaging and bimodal image-guided sentinel lymph node mapping. J Am Chem Soc. 2011; 133:5508–5515. [PubMed: 21428437]
32. Chou S-W, Shau Y-H, Wu P-C, Yang Y-S, Shieh D-B, Chen C-C. In vitro and in vivo studies of FePt nanoparticles for dual modal CT/MRI molecular imaging. J Am Chem Soc. 2010; 132(38): 13270–13278. [PubMed: 20572667]
33. Pan D, Schirra CO, Senpan A, Schmieder AH, Stacy AJ, Roessl E, Thran A, Wickline SA, Proska R, Lanza GM. An early investigation of ytterbium nanocolloids for selective and quantitative "multicolor" spectral CT imaging. ACS Nano. 2012; 6(4):3364–3370. [PubMed: 22385324]
34. Xing H, Bu W, Zhang S, Zheng X, Li M, Chen F, He Q, Zhou L, Peng W, Hua Y, Shi J. Multifunctional nanoprobes for upconversion fluorescence, MR and CT trimodal imaging. Biomaterials. 2012; 33:1079–1089. [PubMed: 22061493]
35. Reginoa CAS, Walbridge S, Bernardo M, Wong KJ, Johnson D, Lonser R, Oldfield E,H, Choyke PL, Brechbiel MW. A dual CT-MR dendrimer contrast agent as a surrogate marker for convection-enhanced delivery of intracerebral macromolecular therapeutic agents. Contrast Media Mol Imaging. 2008; 3:2–8. [PubMed: 18335478]
36. Carrascosa P, Capunay C, Deviggiano A, Bettinotti M, Goldsmit A, Tajer C, Carrascosa J, Garcia MJ. Feasibility of 64-slice gadolinium-enhanced cardiac CT for the evaluation of obstructive coronary artery disease. Heart. 2010; 96(19):1543–1549. [PubMed: 20406770]
37. Javier DJ, Nitin N, Levy M, Ellington A, Richards-Kortum R. Aptamer-targeted gold nanoparticles as molecular-specific contrast agents for reflectance imaging. Bioconjugate Chem. 2008; 19(6): 1309–1312.
38. van Tilborg GAF, Vucic E, Strijkers GJ, Cormode DP, Mani V, Skajaa T, Reutelingsperger CPM, Fayad ZA, Mulder WJM, Nicolay K. Annexin A5-functionalized bimodal nanoparticles for MRI and fluorescence imaging of atherosclerotic plaques. Bioconjugate Chem. 2010
39. Nahrendorf M, Jaffer FA, Kelly KA, Sosnovik DE, Aikawa E, Libby P, Weissleder R. Noninvasive vascular cell adhesion molecule-1 imaging identifies inflammatory activation of cells in atherosclerosis. Circulation. 2006; 114:1504–1511. [PubMed: 17000904]
40. Pan D, Roessl E, Schlomka J-P, Caruthers SD, Senpan A, Scott MJ, Allen JS, Zhang H, Hu G, Gaffney PJ, Choi ET, Rasche V, Wickline SA, Proksa R, Lanza GM. Computed tomography in color: nanoK-enhanced spectral CT molecular imaging. Angew Chem Int Ed. 2010; 49:9635–9639.
41. Alric C, Taleb J, Le Duc G, Mandon C, Billotey C, Le Meur-Herland A, Brochard T, Vocanson F, Janier M, Perriat P, Roux S, Tillement O. Gadolinium chelate coated gold nanoparticles as contrast

agents for both X-ray computed tomography and magnetic resonance imaging. J Am Chem Soc. 2008; 130(18):5908–5915. [PubMed: 18407638]

42. Lee J-S, Green JJ, Love KT, Sunshine J, Langer R, Anderson DG. Gold, poly(beta-amino ester) nanoparticles for small interfering RNA delivery. Nano Lett. 2009; 9(6):2402–2406. [PubMed: 19422265]
43. Libutti SK, Paciotti GF, Byrnes AA, Alexander HR, Gannon WE, Walker M, Seidel GD, Yuldasheva N, Tamarkin L. Phase I and pharmacokinetic studies of CYT-6091, a novel PEGylated colloidal gold-rhTNF nanomedicine. Clin Cancer Res. 2010; 16(24):6139–6149. [PubMed: 20876255]
44. Cormode DP, Roessl E, Thran A, Skajaa T, Gordon RE, Schlomka JP, Fuster V, Fisher EA, Mulder WJM, Proksa R, Fayad ZA. Atherosclerotic plaque composition: analysis with multicolor CT and targeted gold nanoparticles. Radiology. 2010; 256(3):774–782. [PubMed: 20668118]
45. Cormode DP, Skajaa T, van Schooneveld MM, Koole R, Jarzyna P, Lobatto ME, Calcagno C, Barazza A, Gordon RE, Zanzonico P, Fisher EA, Fayad ZA, Mulder WJM. Nanocrystal core high-density lipoproteins: A multimodal molecular imaging contrast agent platform. Nano Lett. 2008; 8(11):3715–3723. [PubMed: 18939808]
46. Torchilin VP, Frank-Kamenetsky MD, Wolf GL. CT visualization of blood pool in rats by using long-circulating, iodine-containing micelles. Acad Radiol. 1999; 6(1):61–65. [PubMed: 9891154]
47. Trubetskoy VS, Gazelle GS, Wolf GL, Torchilin VP. Block-copolymer of polyethylene glycol and polylysine as a carrier of organic iodine: Design of long-circulating particulate contrast medium for X-ray computed tomography. J Drug Targ. 1997; 4(6):381–388.
48. Kinsella JM, Jimenez RE, Karmali PP, Rush AM, Kotamraju VR, Gianneschi NC, Ruoslahti E, Stupack D, Sailor MJ. X-ray computed tomography imaging of breast cancer by using targeted peptide-labeled bismuth sulfide nanoparticles. Angew Chem Int Ed. 2011; 50(51):12308–12311.
49. Cai QY, Kim SH, Choi KS, Kim SY, Byun SJ, Kim KW, Park SH, Juhng SK, Yoon KH. Colloidal gold nanoparticles as a blood-pool contrast agent for x-ray computed tomography in mice. Invest Radiol. 2007; 42(12):797–806. [PubMed: 18007151]
50. Mukundan S, Ghaghada KB, Badea CT, Kao C-Y, Hedlund LW, Provanzale JM, Johnson GA, Chen E, Bellamkonda RV, Annapragada A. A liposomal nanoscale contrast agent for preclinical CT in mice. Am J Roentgenol. 2006; 186:300–307. [PubMed: 16423931]
51. Arifin DR, Long CM, Gilad AA, Alric C, Roux S, Tillement O, Link TW, Arepally A, Bulte JWM. Trimodal gadolinium-gold microcapsules containing pancreatic islet cells restore normoglycemia in diabetic mice and can be tracked by using US, CT, and positive-contrast MR imaging. Radiology. 2011; 260(3):790–798. [PubMed: 21734156]
52. Schlomka JP, Roessl E, Dorscheid R, Dill S, Martens G, Istel T, Baumer C, Herrmann C, Steadman R, Zeitler G, Livne A, Proksa R. Experimental feasibility of multi-energy photon-counting K-edge imaging in pre-clinical computed tomography. Phys Med Biol. 2008; 53(15): 4031–4047. [PubMed: 18612175]
53. Stacul F, van der Molen AJ, Reimer P, Webb JAW, Thomsen HS, Morcos SK, Almen T, Aspelin P, Bellin MF, Clement O, Heinz-Peer G. Contrast Media Safety Comm E. Contrast induced nephropathy: updated ESUR Contrast Media Safety Committee guidelines. Eur Radiol. 2011; 21(12):2527–2541. [PubMed: 21866433]
54. Goodman LR. The Beatles, the Nobel prize, and CT scanning of the chest. Radiol Clin of N Am. 2010; 48(1):1–7. [PubMed: 19995626]
55. Kulkarni NM, Uppot RN, Eisner BH, Sahani DV. Radiation dose reduction at multidetector CT with adaptive statistical iterative reconstruction for evaluation of urolithiasis: How low can we go? Radiology. 2012; 265(1):158–166. [PubMed: 22891359]
56. Diekmann S, Siebert E, Juran R, Roll M, Deeg W, Bauknecht HC, Diekmann F, Klingebiel R, Bohner G. Dose exposure of patients undergoing comprehensive stroke imaging by multidetector row CT: Comparison of 320-detector row and 64-detector row CT scanners. American Journal of Neuroradiology. 2010; 31(6):1003–1009. [PubMed: 20110373]
57. Earls JP, Berman EL, Urban BA, Curry CA, Lane JL, Jennings RS, McCulloch CC, Hsieh J, Londt JH. Prospectively gated transverse coronary CT angiography versus retrospectively gated helical

technique: Improved image quality and reduced radiation dose. Radiology. 2008; 246(3):742–753. [PubMed: 18195386]

58. Zheng G, Chen J, Li H, Glickson JD. Rerouting lipoprotein nanoparticles to selected alternate receptors for the targeted delivery of cancer diagnostic and therapeutic agents. Proc Natl Acad Sci USA. 2005; 102(49):17757–17762. [PubMed: 16306263]
59. Smith-Bindman R, Miglioretti DL, Johnson E, Lee C, Feigelson HS, Flynn M, Greenlee RT, Kruger RL, Hornbrook MC, Roblin D, Solberg LI, Vanneman N, Weinmann S, Williams AE. Use of diagnostic imaging studies and associated radiation exposure for patients enrolled in large integrated health care systems, 1996-2010. J Am Med Assoc. 2012; 307(22):2400–2409.
60. Sprawls, P. Physical principles of medical imaging. Aspen Publishers; Rockville, USA: 1987.
61. Galper MW, Saung MT, Fuster V, Roessl E, Thran A, Proksa R, Fayad ZA, Cormode DP. Effect of computed tomography scanning parameters on gold nanoparticle and iodine contrast. Invest Radiol. 2012; 47(8):475–481. [PubMed: 22766909]
62. Jackson PA, Rahman WNWA, Wong CJ, Ackerly T, Geso M. Potential dependent superiority of gold nanoparticles in comparison to iodinated contrast agents. Eur J Radiol. 2010; 75(1):104–109. [PubMed: 19406594]
63. Saraste A, Nekolla SG, Schwaiger M. Cardiovascular molecular imaging: an overview. Cardiovasc Res. 2009; 83(4):643–652. [PubMed: 19553359]
64. Molday RS, Mackenzie D. Immunospecific ferromagnetic iron-dextran reagents for the labeling and magnetic separation of cells. J Immun Methods. 1982; 52:353–367.
65. Cormode DP, Fayad ZA. Spectral Hounsfield units-a new radiological concept. European Radiology. 2013; 23(3):640–641. [PubMed: 22971961]
66. Hurrell AH, Butler APH, Cook NJ, Butler PH, Ronaldson JP, Zainon R. Spectral Hounsfield units: a new radiological concept. Eur Radiol. 2012; 22:1008–1013. [PubMed: 22134894]
67. Slowing II, Trewyn BG, Lin VSY. Mesoporous silica nanoparticles for intracellular delivery of membrane-impermeable proteins. J Am Chem Soc. 2007; 129(28):8845–8849. [PubMed: 17589996]
68. Lanza GM, Winter PM, Caruthers SD, Hughes MS, Cyrus T, Marsh JN, Neubauer AM, Partlow KC, Wickline SA. Nanomedicine opportunities for cardiovascular disease with perfluorocarbon nanoparticles. Nanomedicine. 2006; 1(3):321–329. [PubMed: 17716162]
69. Cormode DP, Jarzyna PA, Mulder WJM, Fayad ZA. Modified natural nanoparticles as contrast agents for medical imaging. Adv Drug Deliv Rev. 2010; 62(3):329–338. [PubMed: 19900496]
70. Cherukuri P, Gannon CJ, Leeuw TK, Schmidt HK, Smalley RE, Curley SA, Weisman RB. Mammalian pharmacokinetics of carbon nanotubes using intrinsic near-infrared fluorescence. Proc Natl Acad Sci USA. 2006; 103(50):18882–18886. [PubMed: 17135351]
71. Yang K, Zhang S, Zhang G, Sun X, Lee S-T, Liu Z. Graphene in mice: ultrahigh in vivo tumor uptake and efficient photothermal therapy. Nano Lett. 2010; 10(9):3318–3323. [PubMed: 20684528]
72. Hill ML, Corbin IR, Levitin RB, Cao WG, Mainprize JG, Yaffe MJ, Zheng G. In vitro assessment of poly-iodinated triglyceride reconstituted low-density lipoprotein: initial steps toward CT molecular imaging. Acad Radiol. 2010; 17(11):1359–1365. [PubMed: 20719547]
73. Mattrey RF. Perfluorooctylbromide - a new contrast agent for CT, sonography, and MR imaging. Am J Roentgenol. 1989; 152(2):247–252. [PubMed: 2643258]
74. Johnsson M, Edwards K. Liposomes, disks, and spherical micelles: Aggregate structure in mixtures of gel phase phosphatidylcholines and poly(ethylene glycol)-phospholipids. Biophys J. 2003; 85(6):3839–3847. [PubMed: 14645073]
75. Bricarello DA, Smilowitz JT, Zivkovic AM, German JB, Parikh AN. Reconstituted lipoprotein: a versatile class of biologically-inspired nanostructures. ACS Nano. 2010; 5(1):42–57. [PubMed: 21182259]
76. McMahon KM, Mutharasan RK, Tripathy S, Veliceasa D, Bobeica M, Shumaker DK, Luthi AJ, Helfand BT, Ardehali H, Mirkin CA, Volpert O, Thaxton CS. Biomimetic high density lipoprotein nanoparticles for nucleic acid delivery. Nano Lett. 2011; 11(3):1208–1214. [PubMed: 21319839]

77. Rensen PCN, de Vrueh RLA, Kuiper J, Bijsterbosch MK, Biessen EAL, van Berkel TJC. Recombinant lipoproteins: lipoprotein-like lipid particles for drug targeting. Adv Drug Deliv Rev. 2001; 47:251–276. [PubMed: 11311995]
78. Ko YT, Kale K, Hartner WC, Papahadjopoulos-Sternberg B, Torchilin VP. Self-assembling micelle-like nanoparticles based on phospholipid–polyethyleneimine conjugates for systemic gene delivery. J Cont Rel. 2009; 133:132–138.
79. Torchilin VP. Micellar nanocarriers: Pharmaceutical perspectives. Pharmaceut Res. 2007; 24(1):1–16.
80. Skajaa T, Cormode DP, Falk E, Mulder WJM, Fisher EA, Fayad ZA. High density lipoprotein-based contrast agents for multimodal imaging of atherosclerosis. Arterioscler Thromb Vasc Biol. 2010; 30(2):169–176. [PubMed: 19815819]
81. Hallouard F, Anton N, Choquet P, Constantinesco A, Vandamme T. Iodinated blood pool contrast media for preclinical X-ray imaging applications - A review. Biomaterials. 2010; 31(24):6249–6268. [PubMed: 20510444]
82. Bakan DA, Longino MA, Weichert JP, Counsell RE. Physicochemical characterization of a synthetic lipid emulsion for hepatocyte-selective delivery of lipophilic compounds: Application to polyiodinated triglycerides as contrast agents for computed tomography. J Pharm Sci. 1996; 85(9): 908–914. [PubMed: 8877877]
83. Dick A, Adam G, Tacke J, Prescher A, Southon TE, Gunther RW. Computed tomography of experimental liver abscesses using a new liposomal contrast agent. Investigative Radiol. 1996; 31(4):194–203.
84. Sachse A, Leike JU, Schneider T, Wagner SE, Rossling GL, Krause W, Brandl M. Biodistribution and computed tomography blood-pool imaging properties of polyethylene glycol-coated iopromide-carrying liposomes. Investigative Radiol. 1997; 32(1):44–50.
85. de Vries A, Custers E, Lub J, van den Bosch S, Nicolay K, Grull H. Block-copolymer-stabilized iodinated emulsions for use as CT contrast agents. Biomaterials. 2010; 31(25):6537–6544. [PubMed: 20541800]
86. Oh KS, Lee S, Na JH, Kim J-Y, Kim D-E, Kim K, Kwon IC, Yuk SH, Jeong SY. Blood-pool multifunctional nanoparticles formed by temperature-induced phase transition for cancer-targeting therapy and molecular imaging. Int J Pharm. 2012; 437:192–202. [PubMed: 22944301]
87. Ding J, Wang Y, Ma M, Zhang Y, Lu S, Jiang Y, Qi C, Luo S, Dong G, Wen S, An Y, Gu N. CT/fluorescence dual-modal nanoemulsion platform for investigating atherosclerotic plaques. Biomaterials. 2013; 34(1):209–216. [PubMed: 23069709]
88. Hallouard F, Anton N, Zuber G, Choquet P, Li X, Arntz Y, Aubertin G, Constantinesco A, Vandamme TF. Radiopaque iodinated nano-emulsions for preclinical X-ray imaging. RSC Adv. 2011; 1(5):792–801.
89. Kong WH, Lee WJ, Cui ZY, Bae KH, Park TG, Kim JH, Park K, Seo SW. Nanoparticulate carrier containing water-insoluble iodinated oil as a multifunctional contrast agent for computed tomography imaging. Biomaterials. 2007; 28(36):5555–5561. [PubMed: 17904632]
90. http://www.art.ca/en/imaging-agents/index.php
91. Ryan PJ, Davis MA, DeGaeta LR, Woda B, Melchior DL. Liposomes loaded with contrast material for image enhancement in computed tomography. Work in progress. Radiology. 1984; 152(3):759–762. [PubMed: 6611564]
92. Havron A, Seltzer SE, Davis MA, Shulkin P. Radiopaque liposomes - a promising new contrast material for computed-tomography of the spleen. Radiology. 1981; 140(2):507–511. [PubMed: 7255729]
93. Seltzer SE, Davis MA, Adams DF, Shulkin PM, Landis WJ, Havron A. Liposomes carrying diatrizoate - characterization of biophysical properties and imaging applications. Investigative Radiol. 1984; 19(2):142–151.
94. http://www.marvalbiosciences.com
95. Ghaghada, Ketan. telephone interview, 8/16/12
96. Zheng JZ, Liu JB, Dunne M, Jaffray DA, Allen C. In vivo performance of a liposomal vascular contrast agent for CT and MR-based image guidance applications. Pharm Res. 2007; 24(6):1193–1201. [PubMed: 17373581]

97. Miyata S, Kawabata S, Hiramatsu R, Doi A, Ikeda N, Yamashita T, Kuroiwa T, Kasaoka S, Maruyama K, Miyatake SI. Computed tomography imaging of transferrin targeting liposomes encapsulating both boron and iodine contrast agents by convection-enhanced delivery to F98 rat glioma for boron neutron capture therapy. Neurosurgery. 2011; 68(5):1380–1387. [PubMed: 21273928]

98. Torchilin VP. PEG-based micelles as carriers of contrast agents for different imaging modalities. Adv Drug Deliv Rev. 2002; 54:235–252. [PubMed: 11897148]

99. Elrod DB, Partha R, Danila D, Casscells SW, Conyers JL. An iodinated liposomal computed tomographic contrast agent prepared from a diiodophosphatidylcholine lipid. Nanomed Nanotechnol. 2009; 5(1):42–45.

100. Yordanov AT, Mollov N, Lodder AL, Woller E, Cloninger M, Walbridge S, Milenic D, Brechbiel MW. A water-soluble triiodo amino acid and its dendrimer conjugate for computerized tomography (CT) imaging. J Serb Chem Soc. 2005; 70(2):163–170.

101. Fu Y, Nitecki DE, Maltby D, Simon GH, Berejnoi K, Raatschen H-J, Yeh BM, Shames DM, Brasch RC. Dendritic iodinated contrast agents with PEG-cores for CT imaging: synthesis and preliminary characterization. Bioconjugate Chem. 2006; 17:1043–1056.

102. Guo R, Wang H, Peng C, Shen MW, Zheng LF, Zhang GX, Shi XY. Enhanced X-ray attenuation property of dendrimer-entrapped gold nanoparticles complexed with diatrizoic acid. J Mater Chem. 2011; 21(13):5120–5127.

103. Criscione JM, Dobrucki LW, Zhuang ZW, Papademetris X, Simons M, Sinusas AJ, Fahmy TM. Development and application of a multimodal contrast agent for SPECT/CT hybrid imaging. Bioconjugate Chem. 2011; 22(9):1784–1792.

104. Mieszawska AJM, Willem JM, Fayad Zahi A. Cormode David P. Multifunctional gold nanoparticles for diagnosis and therapy of disease. Mol Pharmaceutics. 2013; 10(4):831–847.

105. Agarwal A, Huang SW, O'Donnell M, Day KC, Day M, Kotov N, Ashkenazi S. Targeted gold nanorod contrast agent for prostate cancer detection by photoacoustic imaging. J Appl Phys. 2007; 102(6)

106. Lytton-Jean AK, Han MS, Mirkin CA. Microarray detection of duplex and triplex DNA binders with DNA-modified gold nanoparticles. Anal Chem. 2007; 79(15):6037–6041. [PubMed: 17614366]

107. Daniel M-C, Astruc D. Gold nanoparticles: assembly, supramolecular chemistry, quantum-size-related properties, and applications toward biology, catalysis, and nanotechnology. Chem Rev. 2004; 104:293–346. [PubMed: 14719978]

108. Dreaden E, Alkilany A, Huang X, Murphy C, El-Sayed M. The golden age: gold nanoparticles for biomedicine. Chem Soc Rev. 2011; 41:2740–2779. [PubMed: 22109657]

109. Murphy CJ, Sau TK, Gole AM, Orendorff CJ, Gao J, Gou L, Hunyadi SE, Li T. Anisotropic metal nanoparticles: synthesis, assembly, and optical applications. J Phys Chem B. 2005; 109:13857–13870. [PubMed: 16852739]

110. Hostetler MJ, Green SJ, Stokes JJ, Murray RW. Monolayers in three dimensions: Synthesis and electrochemistry of omega-functionalized alkanethiolate-stabilized gold cluster compounds. J Am Chem Soc. 1996; 118(17):4212–4213.

111. Thakor AS, Jokerst J, Zavaleta C, Massoud TF, Gambhir SS. Gold nanoparticles: a revival in precious metal administration to patients. Nano Lett. 2011; 11:4029–4036. [PubMed: 21846107]

112. Pilot Study of AuroLase(tm) Therapy in Refractory and/or Recurrent Tumors of the Head and Neck. http://clinicaltrialsgov/ct2/show/NCT00848042 Clinical trial identifier: NCT00848042

113. Plasmonic Nanophotothermic Therapy of Atherosclerosis (NANOM). http://clinicaltrialsgov/ct2/show/NCT01270139 Clinical trial identifier: NCT01270139

114. Plasmonic Photothermal and Stem Cell Therapy of Atherosclerosis Versus Biodegradable Stenting (NANOM2). http://clinicaltrialsgov/ct2/show/NCT01436123 Clinical trial identifier: NCT01436123

115. Hainfeld JF, Slatkin DN, Focella TM, Smilowitz HM. Gold nanoparticles: a new X-ray contrast agent. Brit J Radiol. 2006; 79:248–253. [PubMed: 16498039]

116. Choi HS, Liu W, Misra P, Tanaka E, Zimmer JP, Ipe BI, Bawendi MG, Frangioni JV. Renal clearance of quantum dots. Nat Biotech. 2007; 25(10):1165–1170.

117. Guo R, Wang H, Peng C, Shen MW, Pan MJ, Cao XY, Zhang GX, Shi XY. X-ray attenuation property of dendrimer-entrapped gold nanoparticles. J Phys Chem C. 2010; 114(1):50–56.
118. Wang H, Zheng LF, Peng C, Guo R, Shen MW, Shi XY, Zhang GX. Computed tomography imaging of cancer cells using acetylated dendrimer-entrapped gold nanoparticles. Biomaterials. 2011; 32(11):2979–2988. [PubMed: 21277019]
119. Peng C, Zheng LF, Chen Q, Shen MW, Guo R, Wang H, Cao XY, Zhang GX, Shi XY. PEGylated dendrimer-entrapped gold nanoparticles for in vivo blood pool and tumor imaging by computed tomography. Biomaterials. 2012; 33(4):1107–1119. [PubMed: 22061490]
120. Kojima C, Umeda Y, Ogawa M, Harada A, Magata Y, Kono K. X-ray computed tomography contrast agents prepared by seeded growth of gold nanoparticles in PEGylated dendrimer. Nanotechnology. 2010; 21(24)
121. Ghann WE, Aras O, Fleiter T, Daniel MC. Syntheses and characterization of lisinopril-coated gold nanoparticles as highly stable targeted CT contrast agents in cardiovascular diseases. Langmuir. 2012; 28(28):10398–10408. [PubMed: 22702239]
122. Kattumuri V, Katti K, Bhaskaran S, Boote EJ, Casteel SW, Fent GM, Robertson DJ, Chandrasekhar M, Kannan R, Katti KV. Gum arabic as a phytochemical construct for the stabilization of gold nanoparticles: In vivo pharmacokinetics and X-ray-contrast-imaging studies. Small. 2007; 3(2):333–341. [PubMed: 17262759]
123. Boote E, Fent G, Kattumuri V, Casteel S, Katti K, Chanda N, Kannan R, Churchill R. Gold nanoparticle contrast in a phantom and juvenile swine: models for molecular imaging of human organs using x-ray computed tomography. Acad Radiol. 2010; 17(4):410–417. [PubMed: 20207313]
124. Mieszawska AJ, Gianella A, Cormode DP, Zhao Y, Meijerink A, Langer R, Farokhzad OC, Fayad ZA, Mulder WJM. Engineering of lipid-coated PLGA nanoparticles with a tunable payload of diagnostically active nanocrystals for medical imaging. Chem Commun. 2012; 48:5835–5837.
125. Sun IC, Eun DK, Na JH, Lee S, Kim I-J, Youn I-C, Ko C-Y, Kim H-S, Lim D, Choi K, Messersmith PB, Park TG, Kim SY, Kwon IC, Kim K, Ahn C-H. Heparin-coated gold nanoparticles for liver-specific CT imaging. Chem Eur J. 2009; 15(48):13341–13347. [PubMed: 19902441]
126. Park J-A, Kim H-K, Kim J-H, Jeong S-W, Jung J-C, Lee G-H, Lee J, Chang Y, Kim T-J. Gold nanoparticles functionalized by gadolinium-DTPA conjugate of cysteine as a multimodal bioimaging agent. Bioorg Med Chem Lett. 2010; 20(7):2287–2291. [PubMed: 20188545]
127. Kim H-K, Jung H-Y, Park J-A, Huh M-I, Jung J-C, Chang Y, Kim T-J. Gold nanoparticles coated with gadolinium-DTPA-bisamide conjugate of penicillamine (Au@GdL) as a T1-weighted blood pool contrast agent. J Mater Chem. 2010; 20(26):5411–5417.
128. Sun HM, Yuan QH, Zhang BH, Ai KL, Zhang PG, Lu LH. Gd-III functionalized gold nanorods for multimodal imaging applications. Nanoscale. 2011; 3(5):1990–1996. [PubMed: 21384042]
129. Durr NJ, Larson T, Smith DK, Korgel BA, Sokolov K, Ben-Yakar A. Two-photon luminescence imaging of cancer cells using molecularly targeted gold nanorods. Nano Lett. 2007; 7(4):941–945. [PubMed: 17335272]
130. Brown AL, Naha PC, Cormode DP, Goforth AM. unpublished.
131. Luo Y, Wang CM, Qiao Y, Hossain M, Ma LY, Su M. In vitro cytotoxicity of surface modified bismuth nanoparticles. J Mater Sci -Mater Med. 2012; 23(10):2563–2573. [PubMed: 22802106]
132. Brown AL, Goforth AM. pH-dependent synthesis and stability of aqueous, elemental bismuth glyconanoparticle colloids: potentially biocompatible x-ray contrast agents. Chem Mater. 2012; 24(9):1599–1605.
133. Ai KL, Liu YL, Liu JH, Yuan QH, He YY, Lu LH. Large-scale synthesis of Bi2S3 nanodots as a contrast agent for in vivo x-ray computed tomography imaging. Adv Mater. 2011; 23(42):4886–4891. [PubMed: 21956662]
134. Perera VS, Hao JH, Gao M, Gough M, Zayalij PY, Flask C, Basilion JP, Huang SD. Nanoparticles of the novel coordination polymer KBi(H2O)(2) Fe(CN)(6).H2O as a potential contrast agent for computed tomography. Inorg Chem. 2011; 50(17):7910–7912. [PubMed: 21797245]

135. Andres-Verges M, Morales MD, Veintemillas-Verdaguer S, Palomares FJ, Serna CJ. Core/shell magnetite/bismuth oxide nanocrystals with tunable size, colloidal, and magnetic properties. Chem Mater. 2012; 24(2):319–324.
136. Wolf GL, Rogowska J, Hanna GK, Halpern EF. Percutaneous CT lymphography with perflubron -imaging efficacy in rabbits and monkeys. Radiology. 1994; 191(2):501–505. [PubMed: 8153329]
137. Mattrey RF, Long DM, Peck WW, Slutsky RA, Higgins CB. Perfluoroctylbromide as a blood pool contrast agent for liver, spleen, and vascular imaging in computed-tomography. J Comput Assist Tomo. 1984; 8(4):739–744.
138. Mattrey RF, Andre M, Campbell J, Mitten R, Multer F, Hackney D, Long DM, Higgins CB. Specific enhancement of intra-abdominal abscesses with perfluoroctylbromide for CT imaging. Investigative Radiol. 1984; 19(5):438–446.
139. Chen F, Huang P, Zhu YJ, Wu J, Zhang CL, Cui DX. The photoluminescence, drug delivery and imaging properties of multifunctional Eu3+/Gd3+ dual-doped hydroxyapatite nanorods. Biomaterials. 2011; 32(34):9031–9039. [PubMed: 21875748]
140. Liu YL, Ai KL, Liu JH, Yuan QH, He YY, Lu LH. A high-performance ytterbium-based nanoparticulate contrast agent for in vivo x-ray computed tomography imaging. Angew Chem Int Ed. 2012; 51(6):1437–1442.
141. Bonitatibus PJ, Torres AS, Goddard GD, FitzGerald PF, Kulkarni AM. Synthesis, characterization, and computed tomography imaging of a tantalum oxide nanoparticle imaging agent. Chem Commun. 2010; 46(47):8956–8958.
142. Bonitatibus PJ, Torres AS, Kandapallil B, Lee BD, Goddard GD, Colborn RE, Marino ME. Preclinical assessment of a zwitterionic tantalum oxide nanoparticle X-ray contrast agent. ACS Nano. 2012; 6(8):6650–6658. [PubMed: 22768795]
143. Torres AS, Bonitatibus PJ, Colborn RE, Goddard GD, FitzGerald PF, Lee BD, Marino ME. Biological performance of a size-fractionated core-shell tantalum oxide nanoparticle x-ray contrast agent. Investigative Radiol. 2012; 47(10):578–587.
144. Sieber MA, Pietsch H, Walter J, Haider W, Frenzel T, Weinmann HJ. A preclinical study to investigate the development of nephrogenic systemic fibrosis: A possible role for gadolinium-based contrast media. Investigative Radiol. 2008; 43(1):65–75.
145. Bonitatibus, Peter. telephone interview, 9/11/12
146. Lavender JP, Goldman JM, Arnot RN, Thakur ML. Kinetics of indium-111 labeled lymphocytes in normal subjects and patients with Hodgkins-disease. Brit Med J. 1977; 2(6090):797–799. [PubMed: 912325]
147. Bulte JWM. In vivo MRI cell tracking: clinical studies. Am J Roentgenol. 2009; 193(2):314–325. [PubMed: 19620426]
148. Engberink RDO, La Blezer E, Hoff EI, van der Pol SMA, van der Toorn A, Dijkhuizen RM, de Vries HE. MRI of monocyte infiltration in an animal model of neuroinflammation using SPIO-labeled monocytes or free USPIO. J Cereb Blood Flow Metab. 2008; 28(4):841–851. [PubMed: 18000513]
149. Bulte JWM, Kraitchman DL. Iron oxide MR contrast agents for molecular and cellular imaging. NMR Biomed. 2004; 17:484–499. [PubMed: 15526347]
150. Arifin DR, Kedziorek DA, Fu Y, Chan KWY, McMahon MT, Weiss CR, Kraitchman DL, Bulte JWM. Microencapsulated cell tracking. NMR Biomed. 2013 online.
151. Barnett BP, Kraitchman DL, Lauzon C, Magee CA, Walczak P, Gilson WD, Arepally A, Bulte JWM. Radiopaque alginate microcapsules for X-ray visualization and immunoprotection of cellular therapeutics. Mol Pharm. 2006; 3(5):531–538. [PubMed: 17009852]
152. Barnett BP, Ruiz-Cabello J, Hota P, Liddel R, Walczak P, Howland V, Chacko VP, Kraitchman DL, Arepally A, Bulte JWM. Fluorocapsules for improved function, immunoprotection, and trimodal visualization of cellular therapeutics with magnetic resonance, ultrasound and X-ray imaging. Radiology. 2010; 258(1):182–191. [PubMed: 20971778]
153. Menk RH, Schultke E, Hall C, Arfelli F, Astolfo A, Rigon L, Round A, Ataelmannan K, MacDonald SR, Juurlink BHJ. Gold nanoparticle labeling of cells is a sensitive method to

investigate cell distribution and migration in animal models of human disease. Nanomed-Nanotechnol. 2011; 7(5):647–654.

154. Winter PM, Shukla HP, Caruthers SD, Scott MJ, Fuhrhop RW, Robertson JD, Gaffney PJ, Wickline SA, Lanza GM. Molecular imaging of human thrombus with computed tomography. Acad Radiol. 2005; 12(S1):S9–13. [PubMed: 16106538]
155. Pan D, Williams TA, Senpan A, Allen JS, Scott MJ, Gaffney PJ, Wickline SA, Lanza GM. Detecting vascular biosignatures with a colloidal, radio-opaque polymeric nanoparticle. J Am Chem Soc. 2009; 131(42):15522–15527. [PubMed: 19795893]
156. Laakkonen P, Porkka K, Hoffman JA, Ruoslahti E. A tumor-homing peptide with a targeting specificity related to lymphatic vessels. Nat Med. 2002; 8(7):751–755. [PubMed: 12053175]
157. Hyafil F, Cornily JC, Feig JE, Gordon R, Vucic E, Amirbekian V, Fisher EA, Fuster V, Feldman LJ, Fayad ZA. Noninvasive detection of macrophages using a nanoparticulate contrast agent for computed tomography. Nat Med. 2007; 13:636–641. [PubMed: 17417649]
158. Popovtzer R, Agrawal A, Kotov NA, Popovtzer A, Balter J, Carey TE, Kopelman R. Targeted gold nanoparticles enable molecular CT imaging of cancer. Nano Lett. 2008; 8(12):4593–4596. [PubMed: 19367807]
159. Wyss C, Schaefer SC, Juillerat-Jeanneret L, Lagopoulos L, Lehr HA, Becker CD, Montet X. Molecular imaging by micro-CT: specific E-selectin imaging. Eur Radiol. 2009; 19(10):2487–2494. [PubMed: 19440717]
160. Eck W, Nicholson AI, Zentgraf H, Semmler W, Bartling S. Anti-CD4-targeted gold nanoparticles induce specific contrast enhancement of peripheral lymph nodes in X-ray computed tomography of live mice. Nano Lett. 2010; 10(7):2318–2322. [PubMed: 20496900]
161. Feuerlein S, Roessl E, Proksa R, Martens G, Klass O, Jeltsch M, Rasche V, Brambs HJ, Hoffmann MHK, Schlomka JP. Multienergy photon-counting K-edge imaging: potential for improved luminal depiction in vascular imaging. Radiology. 2008; 249(3):1010–1016. [PubMed: 18849505]
162. Anderson NG, Butler AP, Scott NJA, Cook NJ, Butzer JS, Schleich N, Firsching M, Grasset R, de Ruiter N, Campbell M, Butler PH. Spectroscopic (multi-energy) CT distinguishes iodine and barium contrast material in MICE. Eur Radiol. 2010; 20(9):2126–2134. [PubMed: 20309554]
163. Ding HJ, Ducote JL, Molloi S. Breast composition measurement with a cadmium-zinc-telluride based spectral computed tomography system. Med Phys. 2012; 39(3):1289–1297. [PubMed: 22380361]
164. Wang XL, Meier D, Taguchi K, Wagenaar DJ, Patt BE, Frey EC. Material separation in x-ray CT with energy resolved photon-counting detectors. Med Phys. 2011; 38(3):1534–1546. [PubMed: 21520865]
165. Alvarez RE, Macovski A. Energy-selective reconstructions in x-ray computed tomography. Phys, Med Biol. 1976; 21:733–744. [PubMed: 967922]
166. Roessl E, Proksa R. K-edge imaging in x-ray computed tomography using multi-bin photon counting detectors. Phys Med Biol. 2007; 52(15):4679–4696. [PubMed: 17634657]
167. Budoff MJ, Dowe D, Jollis JG, Gitter M, Sutherland J, Halamert E, Scherer M, Bellinger R, Martin A, Benton R, Delago A, Min JK. Diagnostic performance of 64-multidetector row coronary computed tomographic angiography for evaluation of coronary artery stenosis in individuals without known coronary artery disease. J Am Coll Cardiol. 2008; 52(21):1724–1732. [PubMed: 19007693]
168. Greenland P, Bonow RO, Brundage BH, Budoff MJ, Eisenberg MJ, Grundy SM, Lauer MS, Post WS, Raggi P, Redberg RF, Rodgers GP, Shaw LJ, Taylor AJ, Weintraub WS. ACCF/AHA 2007 Clinical Expert Consensus Document on coronary artery calcium scoring by computed tomography in global cardiovascular risk assessment and in evaluation of patients with chest pain - A report of the American College of Cardiology Foundation Clinical Expert Consensus Task Force (ACCF/AHA writing committee to update the 2000 expert consensus document on electron beam computed tomography) developed in collaboration with the Society of Atherosclerosis Imaging and Prevention and the Society of Cardiovascular Computed Tomography. Circulation. 2007; 115(3):402–426. [PubMed: 17220398]

169. Naghavi M, Libby P, Falk E, Casscells SW, Litovsky S, Rumberger J, Badimon JJ, Stefanadis C, Moreno P, Pasterkamp G, Fayad Z, Stone PH, Waxman S, Raggi P, Madjid M, Zarrabi A, Burke A, Yuan C, Fitzgerald PJ, Siscovick DS, de Korte CL, Aikawa M, Airaksinen KEJ, Assmann G, Becker CR, Chesebro JH, Farb A, Galis ZS, Jackson C, Jang IK, Koenig W, Lodder RA, March K, Demirovic J, Navab M, Priori SG, Rekhter MD, Bahr R, Grundy SM, Mehran R, Colombo A, Boerwinkle E, Ballantyne C, Insull W, Schwartz RS, Vogel R, Serruys PW, Hansson GK, Faxon DP, Kaul S, Drexler H, Greenland P, Muller JE, Virmani R, Ridker PM, Zipes DP, Shah PK, Willerson JT. From vulnerable plaque to vulnerable patient - A call for new definitions and risk assessment strategies: Part I. Circulation. 2003; 108(14):1664–1672. [PubMed: 14530185]

170. Roessl E, Brendel B, Engel K-J, Schlomka J-P, Thran A, Proksa R. Sensitivity of photon-counting based K-edge imaging in X-ray computed tomography. IEEE Transactions On Medical Imaging. 2011; 30(9):1678–1690. [PubMed: 21507770]

171. Gottlieb I, Lima JAC. Screening high-risk patients with computed tomography angiography. Circulation. 2008; 117:1318–1332. [PubMed: 18332277]

172. Kramer C. All high-risk patients should not be screened with computed tomographic angiography. Circulation. 2008; 117:1333–1339. [PubMed: 18332278]

173. Mulder WJM, Strijkers GJ, van Tilborg GAF, Griffioen AW, Nicolay K. Lipid-based nanoparticles for contrast-enhanced MRI and molecular imaging. NMR Biomed. 2006; 19(1): 142–164. [PubMed: 16450332]

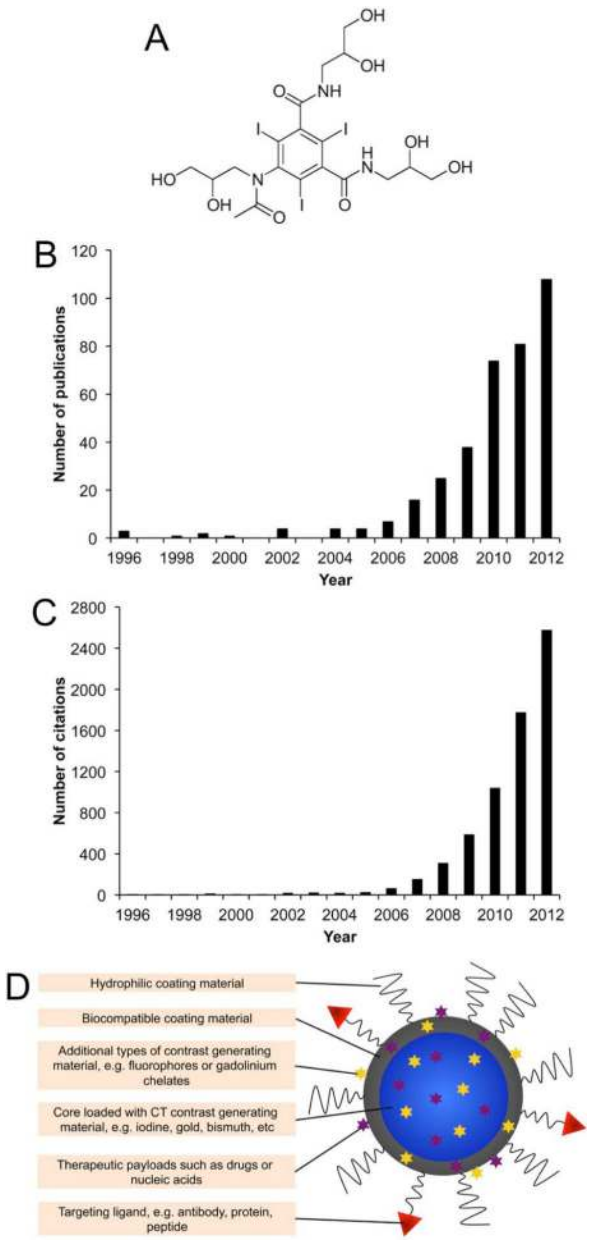

Figure 1.

A) The chemical structure of iohexol. Graphs of the increase in B) publications and C) citations in the area of computed tomography and nanoparticles over the past 17 years. Data acquired from a search of 'computed tomography' refined by 'nanoparticles' in the Web of Science database. The data is reproduced with permission from Thomson Reuters. D) Generalized schematic depiction of CT nanoparticle contrast agent.

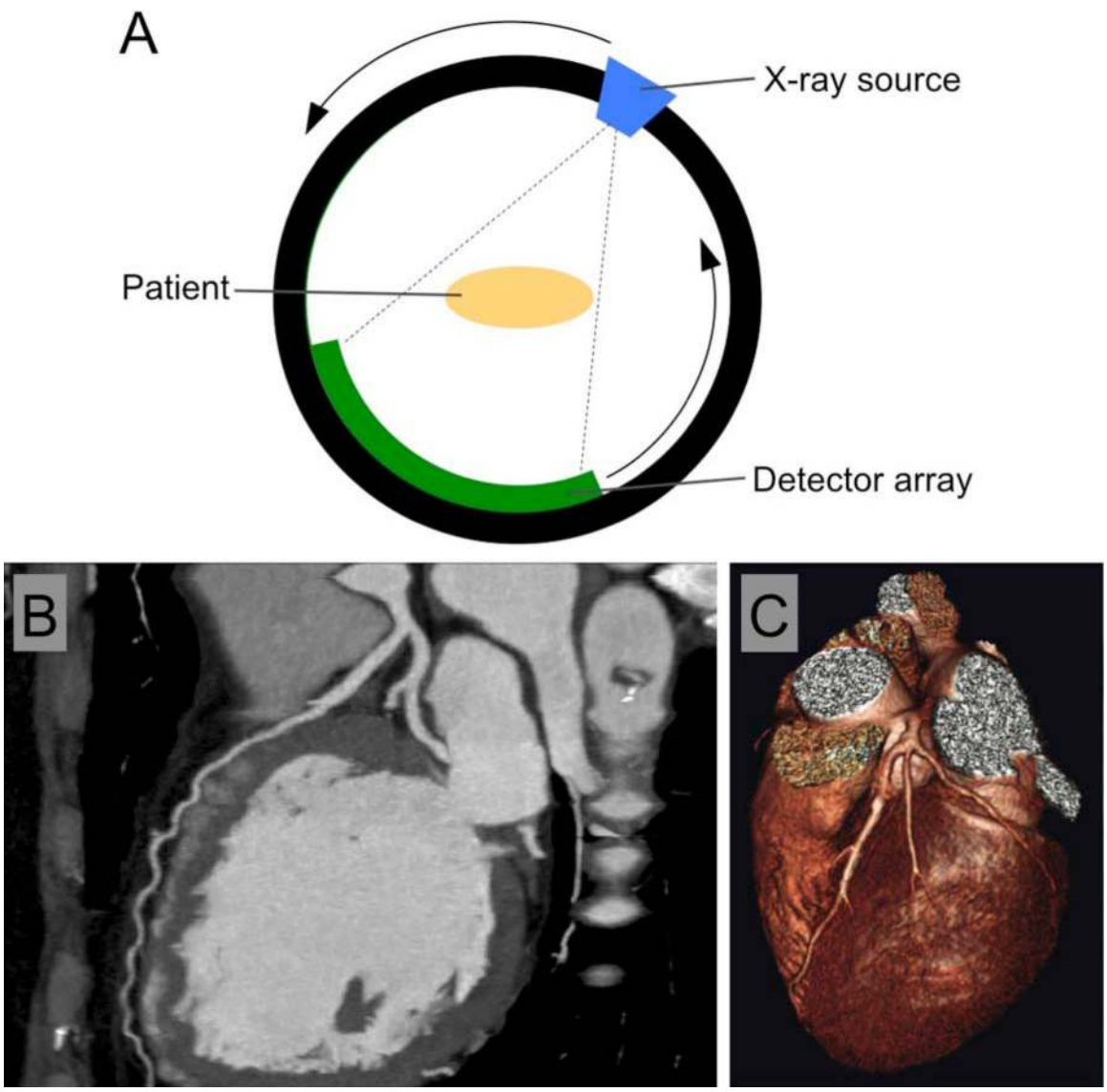

Figure 2.
A) A schematic of a CT scanner. B) A grayscale image of the heart of a patient who had been injected with an iodinated contrast agent. C) A false color, 3D-rendered image of the heart of a patient. Images reproduced with permission from (171,172).

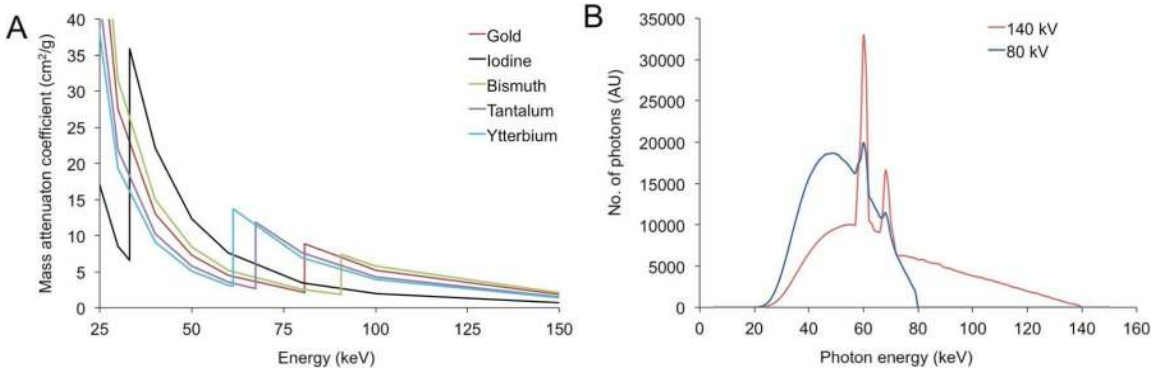

Figure 3.

A) Mass attenuation coefficients of a variety of elements. Data downloaded from (64). B) Photon energy distribution generated from the X-ray tube of a CT scanner run at 80 or 140 kV. Adapted with permission from (61).

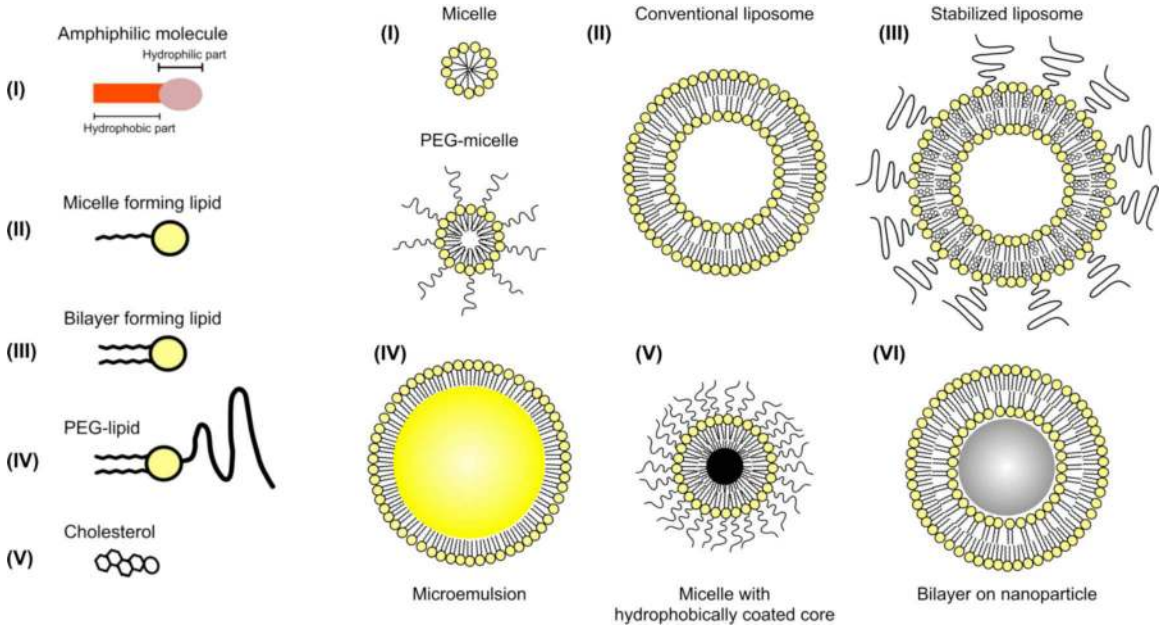

Figure 4.
Schematic depiction of a number of nanoparticle types formed from aggregates of lipids. Reproduced with permission from reference (173).

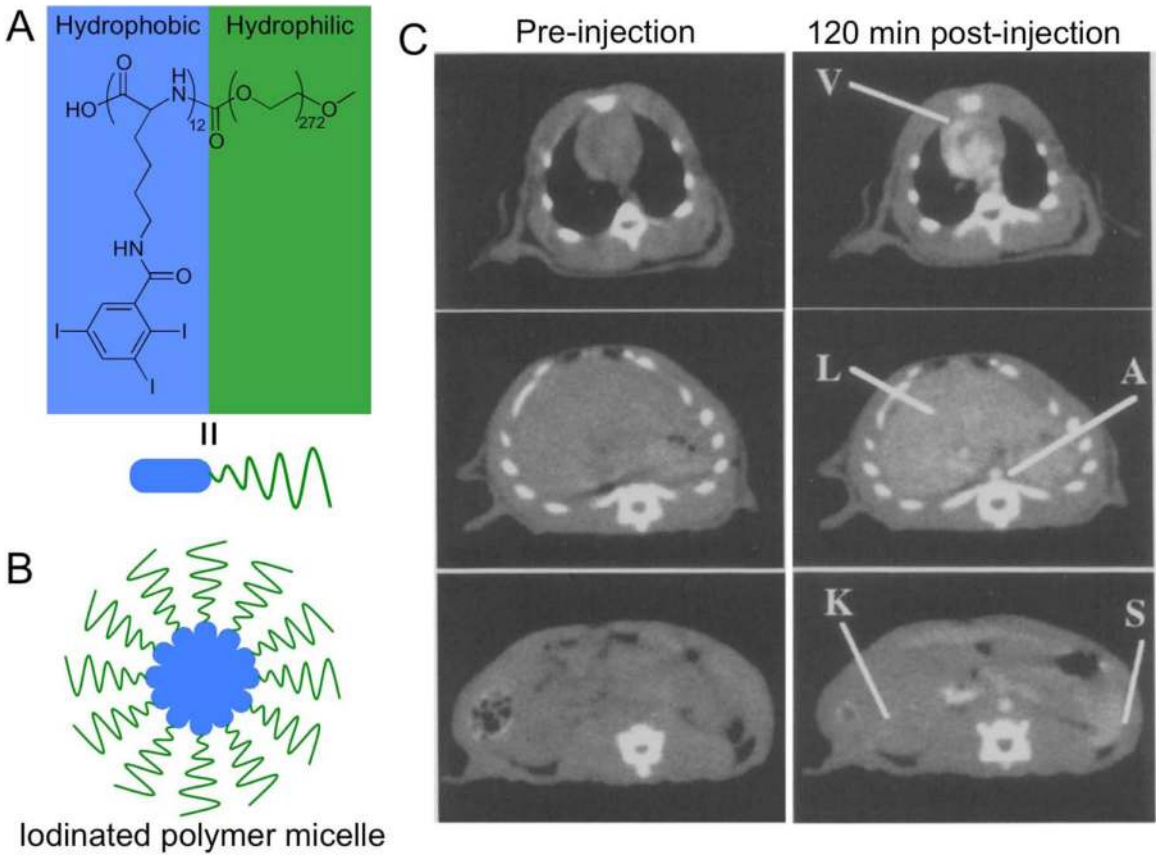

Figure 5.

A) chemical structure of an iodinated polymeric lipid. B) Schematic depiction of a micelle formed from the iodinated polymeric lipid. C) CT images of a rat at the level of the heart, liver and spleen before and after injection with the iodinated micelles. Images reproduced with permission from reference (46).

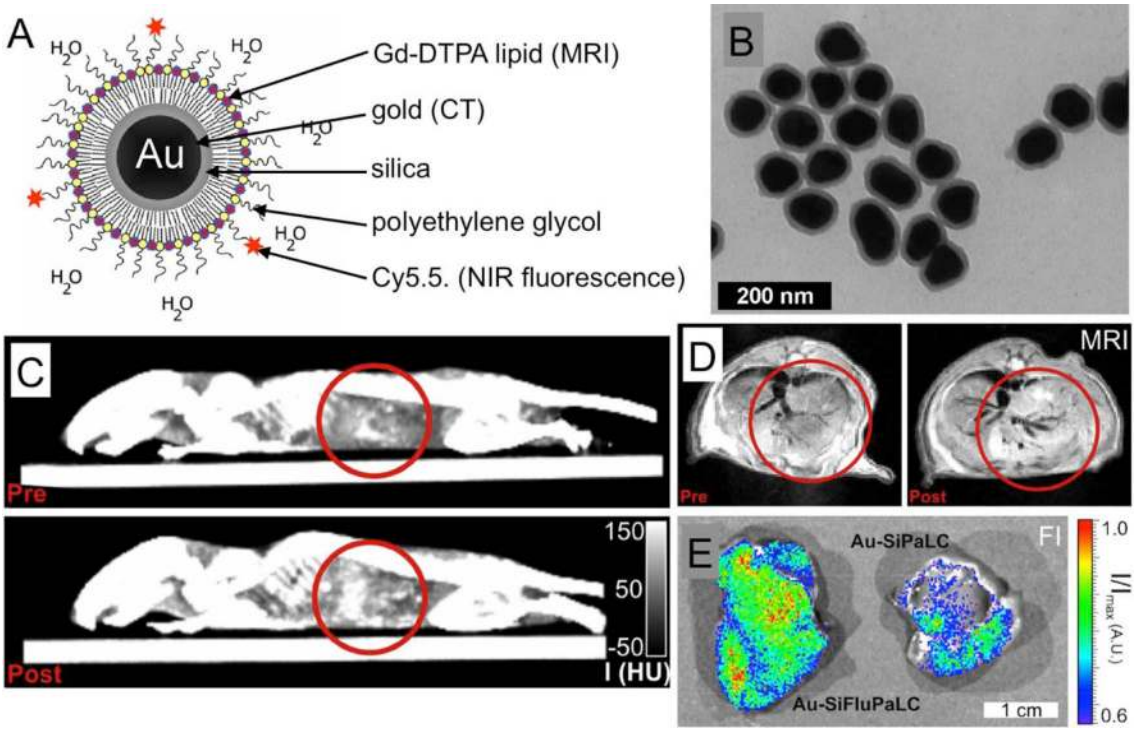

Figure 6.

A) Schematic depiction of a CT/MRI/fluorescence active, micelle-based gold nanoparticle contrast agent. B) Transmission electron microscopy characterization of the nanoparticles. C) CT and D) MR images of a mouse liver pre- and 24 hours post-injection with the gold nanoparticles. E) Fluorescence imaging of the livers of mice injected with either fluorescent (left) or non-fluorescent (right) gold nanoparticles. Figure adapted with permission from (28).

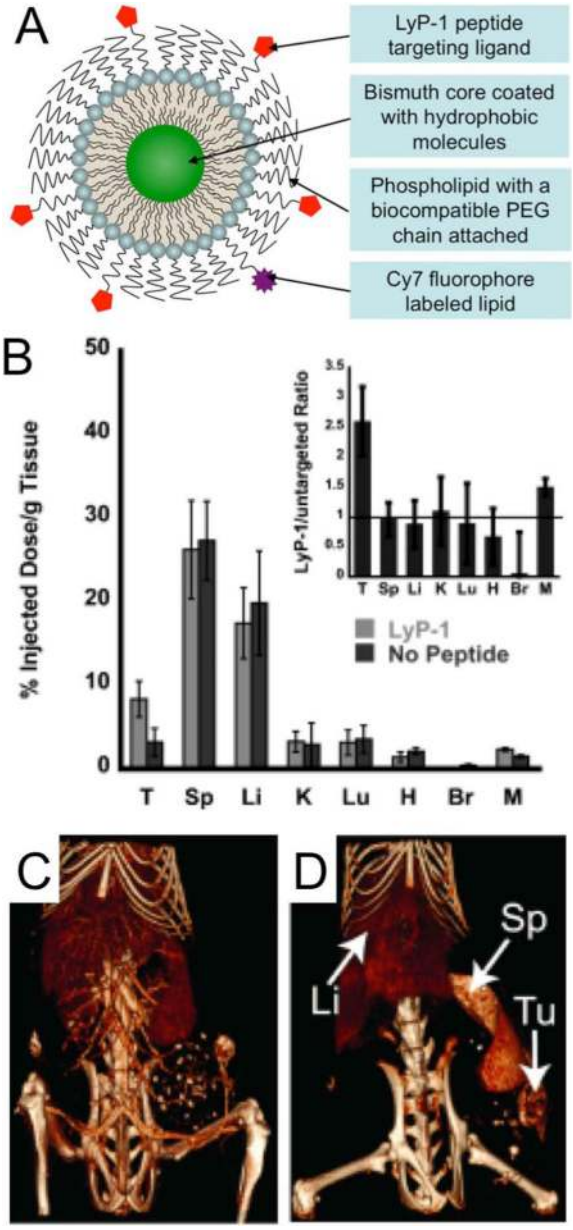

Figure 7.

A) Schematic depiction of the structure of a micelle-based, targeted bismuth core nanoparticle. B) Biodistribution of targeted and non-targeted nanoparticle formulations at 24 hours post-injection. T=tumor, Sp=spleen, Li=liver, K=kidney, Lu=lungs, H = heart, Br = brain, M = muscle. CT images acquired C) immediately and D) 24 hours post-injection of targeted nanoparticles. Figure adapted with permission from (48).

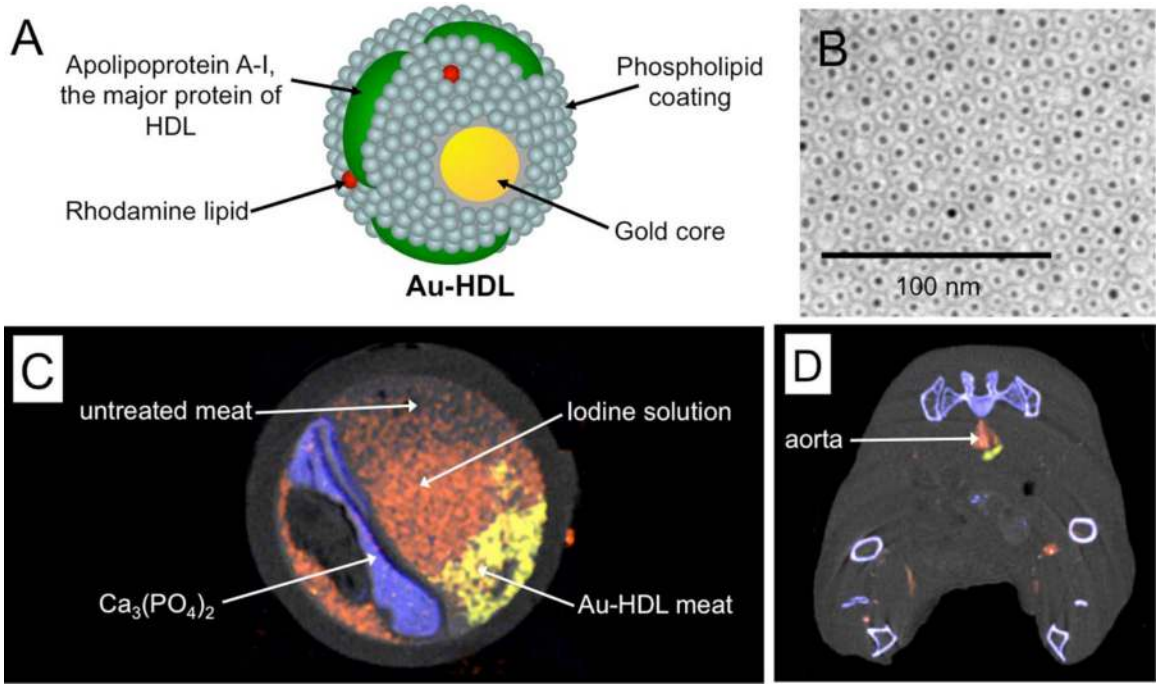

Figure 8.

A) Structure of Au-HDL, a macrophage targeted CT contrast agent. B) Negative stain transmission electron microscopy characterization of the nanoparticle. C) Spectral CT image of an artery phantom. D) Spectral CT image of an atherosclerotic mouse acquired 24 hours after injection with Au-HDL and directly after injection of an iodine nanoemulsion. In C) and D) gold (yellow), iodine (red) and photoelectric (blue) images are overlaid on a Compton image (greyscale). Images reproduced with permission from (44).